EUROPEAN ORGANIZATION FOR NUCLEAR RESEARCH

TWO-NEUTRON EMISSION INDUCED BY STOPPED π^- ON ^{9}Be, ^{10}B, AND ^{12}C *)

B. Bassalleck, W.-D. Klotz, F. Takeutchi**), and H. Ullrich

Kernforschungszentrum und Universität Karlsruhe
Institut für Experimentelle Kernphysik, Fed. Rep. Germany
and CERN, Geneva, Switzerland

and

M. Furić***)

CERN, Geneva, Switzerland

ABSTRACT

The $(\pi^-,2n)$ process has been studied in a kinematically complete experiment on three neighbouring 1p-shell nuclei. Distributions of excitation energy of the residual nuclei, of recoil momentum, of the angle between the emitted neutrons, and the angle between the sum and the difference of the neutron momenta have been measured. From the excitation spectra a striking analogy with (p,2p) data has been found in the region of p-shell nucleon removal. The possibility of s-shell nucleon removal has been investigated. The data are compared with theoretical predictions.

Nucleon reaction $(\pi^-,2n)$ on ^{9}Be, ^{10}B, and ^{12}C, E = 0 measured rate (En_1,En_2,ω); excitation spectra for residual nuclei deduced, recoil momentum distributions extracted.

Geneva - 28 March 1977

(Submitted to Physical Review)

*) Work supported in part by the Bundesministerium für Forschung and Technologie of the Federal Republic of Germany.

**) Present address: Department of Physics, Kyoto Sangyo University, Kamigamo-Motoyama, Kyoto, Japan.

***) On leave of absence from Institute R. Bošković, Zagreb, Yugoslavia.

1. INTRODUCTION

In light nuclei the pion absorption with the subsequent back-to-back emission of a nucleon pair proceeds very strongly via the quasi-free mechanism. The coincident detection and energy measurement of both nucleons permit a complete determination of the kinematical properties for the absorbing pair. This offers an excellent opportunity to study separation energies, momentum distributions, and angular momenta of the two nucleons involved[1]. Such experiments are also expected to yield information about the πNN interaction itself, and its dependence on the different quantum states of the NN-combinations inside nuclei.

The theoretical treatment of the pion absorption in nuclei presents a major problem. The following aspects have to be taken into account simultaneously: a) short-range correlations between the nucleons in the initial state; b) the interaction between three and more particles in the final state; c) a proper description of the pion absorption dynamics; and, d) realistic wave functions for the absorbing nucleus. So far only two published calculations include (a), (b), and (c). They differ in the approach to the final state. While Morris and Weber[2] use the coupled channel method with realistic interactions, Garcilazo and Eisenberg[3] solve the Faddeev equation with separable potentials. However, experimentally observable features such as excitation spectra of residual nuclei and momentum distributions are strongly influenced by (d). Consequently our data will be compared with calculations using more realistic nuclear wave functions. We use results of Kopaleishvili et al.[4] who consider only the nucleon-nucleon interaction in the final state, but include (c) and (d). In addition, we use the tabulated coefficients of fractional parentage (c.f.p.) for the two-nucleon removal of Cohen and Kurath[5] (CK) and of Balashov et al.[6] (BBR).

On the experimental side, the results with best energy resolution until recently could be obtained with $(\pi^+,2p)$ measurements[7,8]. In most cases, however, the insufficient energy resolution or inadequate statistics hampered the identification of the discrete final states. The resolution of the existing $(\pi^-,2n)$ measurements[9,10] was at least a factor of 3 lower than that of the $(\pi^+,2p)$ experiments. Owing to charge symmetry $(\pi^-,2n)$ and $(\pi^+,2p)$ reactions should lead to identical states in the same residual nucleus if the quasi-free mechanism is the dominant one and if the kinematical conditions are identical for both experiments. The latter condition is not fulfilled *a priori*, since $(\pi^+,2p)$ studies are performed with pions in flight, while in $(\pi^-,2n)$ experiments pion absorption occurs "at rest". This causes a difference not only in pion energy but possibly also in the pion angular momentum relative to the nucleon pair. A comparison between $(\pi^+,2p)$ and $(\pi^-,2n)$ measurements with equivalent accuracy can therefore test the basic assumptions on the mechanism, and also investigate the influence of the

initial pion state on the experimental results, especially on the excitation spectra. A difference between the two reactions had been already reported for the target ^{14}N [11].

In the $(\pi^-,2n)$ reactions on 1p-shell nuclei, strong peaks observed in the excitation spectra for the residual nuclei are so far mainly attributed to nucleon removal from the p-shell. Only for the lithium targets has a large contribution from the s-shell nucleons also been identified[7,10,12]. Evidence for the two-hole states in the p-shell and, separately, in the s-shell was reported in the reaction $^{12}C(\pi^-,2n)^{10}B$ [9]. However, the peak due to the holes in the s-shell was not observed in an experiment with higher resolution on the analogous $(\pi^+,2p)$ reaction[7].

In our experiment we use large-area position-sensitive neutron counters with subnanosecond time resolution. They allow the study of the $(\pi^-,2n)$ reaction with energy resolution[13] comparable to or better than that of the existing $(\pi^+,2p)$ data. At the same time, these counters offer rather large solid angles. The targets ^9Be, ^{10}B, and ^{12}C were used to search systematically for the evidence of the inner shell absorption in the nuclei close to the lithium isotopes. Where possible, we have made comparisons with existing $(\pi^+,2p)$ data and with theoretical predictions.

2. CONCEPTS RELEVANT FOR DATA INTERPRETATION

Figure 1 shows the kinematical variables which are used. In the case of the absorption of stopped π^- followed by a three-body disintegration, there are three independent variables. For a given excitation energy of the residual nucleus E_x, p, and q are related by the energy conservation. So the combinations like q and ω, or q and θ, together with E_x, form a complete set of variables to describe the kinematics. The importance of the θ distributions has been pointed out by Koltun[14].

In the quasi-free description of the $(\pi^-,2n)$ reaction, we assume that the pion is absorbed by a neutron-proton pair in the target. In the initial state, the angular momentum of the centre of mass of the pair and of each nucleon with respect to the centre of mass of the target, are L, ℓ_1, and ℓ_2, respectively. The total angular momentum Λ is written as $\Lambda = \ell_1+\ell_2 = L+\ell$, where ℓ denotes the relative angular momentum of the nucleons.

In the following we assume that the pion is mainly absorbed by a pair in relative s-state, i.e. $\ell = 0$, and we have $L = \Lambda$. For p^2 removal, i.e. for the removal of two nucleons from the p-shell, we have $\ell_1 = \ell_2 = 1$ and therefore $L = 0$ or 2, and in both cases the parity of the residual state is the same as that of the target. It should be noted that the n-p pair can be in a spin triplet, isospin singlet, or a spin singlet, isospin triplet state. For L = 0 the energy

conservation in the shell model allows the admixture of the following two combinations:

$$\text{a) } 2S\ (\mathcal{N} = 1,\ L = 0) \times 1s\ (n = 0,\ \ell = 0)$$

$$\text{b) } 1S\ (\mathcal{N} = 0,\ L = 0) \times 2s\ (n = 1,\ \ell = 0)\ ,$$

where $\mathcal{N}$ and n are the principal quantum numbers associated with the c.m. motion and the relative motion of the two nucleons, respectively. In contrast to the $(\pi,2N)$ reactions, (b) is suppressed in the case of two-nucleon transfer or quasi-free deuteron knockout reactions, because the removed nucleon pair is not in the lowest energy state. For $\Lambda = 2$, under the assumption of $\ell = 0$, there is only one combination possible:

$$\text{c) } 1D\ (\mathcal{N} = 0,\ L = 2) \times 1s\ (n = 0,\ \ell = 0)\ ^{*)}\ .$$

For the removal of an s-p pair, we have L = 1, and the possible combination is

$$\text{d) } 1P\ (\mathcal{N} = 0,\ L = 1) \times 1s\ (n = 0,\ \ell = 0)\ .$$

The parity of the residual state is different from that of the target nucleus. For the removal of an s^2 pair, we have L = 0, and the only possible combination is:

$$\text{e) } 1S\ (\mathcal{N} = 0,\ L = 0) \times 1s\ (n = 0,\ \ell = 0)\ .$$

The parity of the residual state is again the same as that of the target.

The q-distribution for a given residual state is dominated by L and $\mathcal{N}$, and is essentially the absolute value squared of the c.m. wave function of the two nucleons in the momentum space. In Fig. 2 we show two measured q-distributions for different n-p pairs with similar separation energies. They are compared with simplified calculations for different $\mathcal{N}$ and L carried out with a square well potential and the corresponding separation energies. It should be mentioned that for the case of L = 0, the width of the distribution is dominated by the separation energy of the pair in the target. Large separation energies correspond to wider distributions.

For the interpretation of the experimentally obtained q-distributions, the following should be considered:

---

*) For the geometrical reason stated later, this component is suppressed. In this case, the admixture of the component (d), $1S\ (\mathcal{N} = 0,\ L = 0) \times 1d\ (n = 0,\ \ell = 2)$, may become important.

i) So as to detect mainly the quasi-free events, our counters are placed at $\omega \sim 180°$, and hence small q is favoured. Levels corresponding to $L \neq 0$ (especially to L = 2) transitions are therefore suppressed in the excitation spectra. In the case of $\Lambda = 2$ transitions, component (d) involving 1S may become more important. However, as 1S also shows a wide q-distribution, we expect a wide distribution for $\Lambda = 2$ for any admixture of (c) and (d).

ii) The shape of the q-distributions can be modified owing to various effects. The distribution for $L \neq 0$ is expected to be zero at q = 0, but the distortion effects caused by initial- and final state interactions tend to fill this dip. Also, if the pions are preferentially absorbed at the nuclear surface, or if the emitted nucleons originating from the inner regions undergo stronger distortions, the contribution of the wave function of the c.m. of the pair at small radii is suppressed. Hence in the resultant q-distributions, the peak position shifts towards small q for $L \neq 0$, and the width becomes smaller for L = 0 [15].

If the process is dominated by short-range correlations, the large-p components of the initial state play the important role. As by energy conservation, large p is related to small q, this effect will enhance the small-q components and hence will have the same result as the preceding effect.

3. EXPERIMENTAL SET-UP AND DATA HANDLING

Negative pions of 70 MeV from the CERN Synchro-cyclotron (SC) low-energy pion channel were stopped in targets of 3-5 g/cm^2 thickness. The experimental set-up is shown in Fig. 3. All counters were plastic scintillators.

The pion stop trigger was obtained from counters I and II before the degrader, counter III and the hodoscope, between the degrader and the target, in coincidence, and counter V in anticoincidence. Counter II, with the dimensions 12 cm × 10 cm × × 1 cm, had a pair of twisted-strip light-guides, two RCA 8850 photomultipliers, and was used as the start counter for the two neutron time-of-flight counters. The time resolution of this counter for 2 MeV pulses was 300 psec. The pulse height of counter III was used to determine the pion stopping point in the target in the beam direction. The hodoscope strips, of 2 cm width each, mounted on Philips 1110 phototubes, served to fix the stopping point in the target in the horizontal direction, perpendicular to the beam. Counter IV was a plastic scintillator of 0.5 mm thickness; it enabled us to reject those pions which stopped in the hodoscope.

The two outgoing neutrons were detected in coincidence with a pair of large-area, position-sensitive, time-of-flight counters, placed 4.5 m from the target. The angle between the centres of the counters was 160°, thus covering an ω-range

from 140° to 180°. The sensitive volume of one neutron counter is 2 m wide × 48 cm high × 9 cm thick, covering a solid angle of 47 msr at a distance of 4.5 m from the target.

To localize the neutron impact point vertically, the counter is subdivided into eight bundles of scintillators, each of 6 cm height. In order to improve the time resolution by localizing the impact point in depth, it is also subdivided into six layers of 1.5 cm thickness each. In total, each counter consists of 48 rods, made of NE 110 plastic scintillator and assembled as indicated in Fig. 3. The development and testing of a prototype counter has been described previously[16]. Two adjacent bundles are viewed by a 56 DVP photomultiplier at each end. The position information along the counter is taken from the time difference between the two photomultipliers. A total of 30 small phototubes (Philips 1110) on each counter show the pattern of the rods that have given a signal for each event.

The time-of-flight information, time difference between the photomultipliers on both sides, pulse heights of the 56 DVP's, and pattern information of all phototubes as well as hodoscope information and counter III pulse-height, were written on tape, event by event, via a CAMAC system and a PDP 8L on-line computer. The pulse-height information from the neutron counters was later used to set a threshold, in the off-line program, and also to remove the residual walk of the ORTEC 473 constant-fraction discriminators used.

A typical time resolution of a neutron counter is 800 psec for 20 MeV electron equivalent pulses, including start counter resolution. This resulted in an excitation energy resolution ΔE_x of 3-6 MeV FWHM, depending on pulse-height threshold, flight path, and on E_x. This resolution is at least a factor of 3 better than in previous $(\pi^-, 2n)$ measurements.

All data were written on magnetic tape and analysed using the CERN CDC 7600. In the off-line analysis, a sufficiently high pulse-height threshold (4-5 MeV electron equivalent) was set to get a uniform efficiency over the whole counter by taking into account the light attenuation in the rods[16]. The efficiency correction was made with the Kurz code[17], which had been tested on the prototype counter in an independent efficiency measurement. All distributions shown are corrected for this effect. Usually, neutrons with kinetic energy below 15 MeV were rejected. Also events from the last 12 cm on each side of the counters were not accepted because of non-uniformity in the effective light-propagation velocity. If the first layer had triggered, and if the measured pulse height and kinetic energy were in a certain relation, then the event was assigned to a charged particle and was rejected. The data have also been corrected for geometrical acceptance in our ω-range between 145° and 180°. The corresponding correction function has been determined for our geometry with high statistical accuracy using a Monte Carlo simulation program.

Within the experimental limitations (E_{kin} > 15 MeV, ω > 145°) our data are therefore free of geometrical bias and can be directly compared with theory. The recoil momentum distributions shown are obtained by dividing the corrected rate by the three-body phase-space factor. For the θ-distributions, q has been restricted to values where there is no reduction in phase space caused by our restricted ω-range. In all figures, the errors given are statistical.

In principle, all our data are available as a function of three independent parameters, as described in Section 2. For practical reasons, however, only one- and two-dimensional distributions are given in this paper.

4. RESULTS AND DISCUSSION -- LOW E_x REGION

4.1 Beryllium-9

So far, the only attempt to study the $^9Be(\pi^-,2n)^7Li$ reactions has been made by Calligaris et al.[10]. Their statistics were poor, however, being based on a total of 145 events, and it was therefore interesting to repeat the measurement with better statistics and good resolution.

Our observed excitation spectrum of the residual ^7Li nucleus is shown in Fig. 4. The spectrum shows a maximum at about 10 MeV and then decreases slowly with increasing excitation energy. The ground state ($3/2^-$) and the 0.48 MeV first excited state ($1/2^-$) are weakly populated. In the α-α-n cluster picture for the ^9Be target, the transition to these levels corresponds to a removal of the weakly bound neutron and a proton from one of the α clusters. The weak rate is therefore probably explained by the rather large distance between the proton and the neutron which absorb the pion. The recoil momentum distribution corresponding to these levels is shown in Fig. 5. It indicates a predominant contribution of L = 0; the half-width is, however, relatively large ($\sim$ 120 MeV/c) for this pair separation energy (see Section 2). It is larger than the corresponding width for higher levels, described later, which have higher separation energy. This fact again supports the assumption of a large distance between the absorbing nucleons and the cluster picture of the ground state of the target nucleus and the two lowest levels of ^7Li.

In the excitation spectrum in Fig. 4 two large peaks in the region between 7 MeV and 11 MeV are visible. As the number of known levels in this region is small, they can be attributed to the levels at 7.47 MeV ($5/2^-$, T = 1/2) and 10.25 MeV ($3/2^-$, T = 1/2). Balashov et al.[6] predict by far the largest spectroscopic factor for the Λ = 0 transition to the members of a $^{2T+1,2S+1}L = {}^{2,4}P$ triplet at about 8-11 MeV. According to Barker[18], the level at 7.47 MeV ($5/2^-$) seems to be the lowest member of this triplet. These facts lead to the conclusion that this transition corresponds to the removal of a spin triplet (T = 0) n-p pair from the

target nucleus. The $\Delta T = 0$ transition is confirmed by the fact that this level is populated in the $^{9}Be(p,^{3}He)^{7}Li$ reaction ($\Delta T = 0,1$) at $E_p = 43.7$ MeV, whereas the mirror level at 7.21 MeV in ^{7}Be is not seen in the $^{9}Be(p,t)^{7}Be$ reaction ($\Delta T = 1$) under the same conditions[19].

The energy of the $^{3}/_{2}^{-}$ member of the $^{2,4}P$ triplet is calculated to be between 8 MeV and 11 MeV [20]. According to Ajzenberg-Selove and Lauritsen[21] the 10.25 MeV level is the only $^{3}/_{2}^{-}$ member of the triplet. Then the large population (seen in Fig. 4) comparable to that of the 7.5 MeV level agrees with the prediction of Balashov et al.[6]. Furthermore, the recoil momentum distributions corresponding to these peaks, shown in Fig. 5 , are rather similar. They both indicate a strong $L = 0$ component, and the half-width is about 90 MeV/c, which is smaller than the width of the q-distribution for the ground and first excited levels already mentioned. Therefore this is in agreement with the $\Lambda = 0$ prediction.

Besides the $^{1}/_{2}^{-}$ member of the $^{2,4}P$ triplet, Balashov et al. predict a large spectroscopic factor also for $[21]^{22}P$ levels at E_x about 16-18 MeV (the numbers in the bracket correspond to the Young scheme). However, except for the 16.8 MeV level, no level is experimentally well established (see Ref. 21), and at the same time no other distinct peak is seen in our excitation spectrum. Therefore, a further comparison of the result with the c.f.p. calculation is difficult.

In conclusion, the largest rates come from the transition to $^{2,4}P$ levels, and the transitions to the ground and first excited states are weak. The analog $(\pi^{+},2p)$ reaction on the same target has been investigated by Favier et al.[7]. Their excitation energy spectrum seems to be similar to ours within their experimental resolution.

4.2 Boron-10

Data on the pion-induced two-nucleon emission with ^{10}B as a target nucleus were obtained for the first time. Figure 6 shows the excitation spectra. Since the residual nucleus ^{8}Be is particle unstable, the four-body break-up contribution in the excitation spectrum is possible even in the ground-state region. In the spectrum without q-windows, two main peaks can be observed at approximately 3 MeV and 19 MeV excitation energy. The momentum distributions for these peaks are shown in Fig. 7. The distribution for the peak at 3 MeV is $\sim$ 150 MeV/c wide. We conclude that it is dominated by a $\Lambda \neq 0$ component. The observed large width of the 3 MeV peak in the excitation energy spectrum can be at least partially explained by the known width of this level in ^{8}Be. The momentum distribution shown in Fig. 7 for the peak around 19 MeV is narrow and it has its maximum in the vicinity of zero momentum, indicating mainly $L = 0$. In Fig. 6 the excitation spectrum restricted to large q-values is also given. It indicates that the broad peak around

19 MeV is a superposition of three peaks at 17, 19, and 22 MeV. The splitting is not visible in the excitation spectrum for low q-values, where only the 19 MeV peak persists. This suggests $\Lambda \neq 0$ for the peaks at 17 and 22 MeV. In the lower curve of Fig. 6 there is also a weak peak visible at 10 MeV, which for the same reasons should correspond to $\Lambda \neq 0$.

The levels with large c.f.p. are also indicated in Fig. 6. When comparing the experimental results with the c.f.p. calculations, several remarks are important. The correspondence between the theoretical and known experimental levels is not completely established, especially in the region of higher excitations. In Fig. 6 the position of the levels is given according to the calculations. The L = 2 transitions are suppressed in our geometry, as discussed previously. The $\Delta T = 1$ transitions can appear only at higher excitations since all the known T = 1 levels in ^{8}Be are above 16 MeV.

At $E_x \sim 3$ MeV both theories[5,6] predict $\Lambda = 2$ contributions in agreement with our data. The calculations differ in the strength for $\Lambda = 2$ transitions to the level at 10 MeV. Cohen and Kurath expect this level to be less populated than the one at 3 MeV, while Balashov et al. predict the opposite. In the region above 16 MeV, strong $\Delta T = 0$, $\Lambda = 0$ transitions are predicted by both Cohen and Kurath and by Balashov et al. which agree with the position of the largest experimental peak at 19 MeV. A $\Delta T = 0$, $\Lambda = 2$ transition is also expected in both calculations at somewhat lower energy than the $\Lambda = 0$ contribution, in agreement with our indication for a level at 17 MeV. None of the $\Delta T = 0$, $\Lambda = 2$ calculations can explain the observed indication of a level around 22 MeV.

Cohen and Kurath expect two $\Delta T = 1$, $\Lambda = 2$ contributions which agree with the excitations at 17 and 22 MeV. It should be noted that only $\Delta T = 1$ calculation explains the excitation around 22 MeV. The largest $\Delta T = 1$, $\Lambda = 0$ transition strength is expected for the level at $\sim$ 18 MeV, in accordance with the position of the main observed peak. However, another $\Delta T = 1$, $\Lambda = 0$ transition, weaker in intensity, is expected around 22 MeV. The middle spectrum in Fig. 6, which emphasizes $\Lambda = 0$ transitions, does not confirm this.

The indication of wide structure at higher energies will be discussed later. The comparison with $(\pi^+,2p)$ or (p,pd) data is not possible, owing to lack of such measurements.

The following summary can be made. In the excitation spectrum of ^{8}Be a $\Lambda = 2$ transition to $E_x \sim 3$ MeV and a $\Lambda = 0$ transition to $E_x \sim 19$ MeV are well identified. Evidence for transitions to additional levels exists at 10, 17 and 22 MeV; $\Lambda = 2$ is assigned to all the corresponding transitions as a dominant component. The isospin assignment for the absorbing nucleon pair is difficult above $E_x \sim 16$ MeV, where $\Delta T = 1$ becomes possible in addition to $\Delta T = 0$. Cohen and

Kurath suggest $\Delta T = 1$ for the $\Lambda = 2$ transition to 22 MeV excitation. For the transition to E_x = 17 MeV and 19 MeV, both isospin values for the nucleon pair are possible.

4.3 Carbon-12

Carbon-12 has often been used as target for $(\pi^-,2n)$ reactions[9,10,22,23] as well as for the analogous $(\pi^+,2p)$ reaction[7]. Ozaki et al.[22] and Nordberg et al.[23] show no excitation energy spectrum, whereas in the case of Calligaris et al.[10] the statistics are very poor. The measurement done by Cheshire and Sobottka[9] had rather bad energy resolution; besides a peak around 5 MeV, the excitation energy spectrum shows a peak around 38 MeV which they have attributed to removal of two s-shell nucleons.

Figure 8 shows our measured excitation energy distribution. Also indicated are levels with large c.f.p. according to calculations for two p-shell nucleon removal[5,6]. The spectrum is dominated by a large peak around 1 MeV, in addition to which there are three more peaks at about 4.5 MeV, 7 MeV, and 12 MeV. Also, there seems to be an indication of a somewhat broader peak at 21-22 MeV.

Cohen and Kurath predict large c.f.p. for transitions to the ground state (3^+, T = 0), first excited state (0.7 MeV, 1^+, T = 0), and second excited state (1.7 MeV, 0^+, T = 1). Our experimental result is compatible with this prediction, as the main contribution lies in the region of $E_x < 5$ MeV. The ground-state transition has $\Lambda = 2$, whereas the other two have $\Lambda = 0$. Our measured q-distribution for this lowest excitation energy range is shown in Fig. 9. It indicates some L = 0 contribution, but the width is significantly larger ($\sim$ 150 MeV/c) than for the targets ^{9}Be or ^{10}B for the same separation energy. As is known from a (π^-,γ) measurement[24], the first three excited states all contribute, and therefore our dominant peak around 1 MeV is very likely composed of ground state plus the first three excited states. Within our energy resolution we cannot give precise numbers for the relative contributions among them.

Also Balashov et al.[6] predict the major strength to be in the low excitation region ($E_x < 3$ MeV) and are thus in qualitative agreement with our result.

The structure around 4.5 MeV can be attributed to the 4.77 MeV level (3^+, T = 0) with some possible contribution from the 3.6 MeV level (2^+, T = 0) and from the levels around 5.1-5.2 MeV. According to the Cohen and Kurath prediction, there should be significant strength in this region for $\Lambda = 2$ transitions. Our measured q-distribution for this E_x part (Fig. 9), is very broad and of different shape than for pure L = 0. From this we conclude that a major $\Lambda = 2$ contribution is possible, in agreement with Cohen and Kurath.

For the peaks above E_x = 6 MeV, no attempt at comparison with known levels has been made. However, it should be emphasized that Cohen and Kurath predict a very large c.f.p. for a $\Lambda = 2$, $\Delta T = 1$ transition to an excitation energy of 7.2 MeV. Indeed we observe a peak around 7 MeV whose q-distribution, shown in Fig. 9, is again very wide with the maximum close to zero momentum. If it is the predicted level, then, in view of the very large predicted c.f.p., it is suppressed compared to the observed $\Lambda = 0$ transition at about 1 MeV. The peak around 12 MeV and the broader structure around 21-22 MeV are discussed later in this paper, in connection with the possibility of s-shell nucleon removal.

The excitation spectrum of the $(\pi^+,2p)$ measurement of Favier et al.[7] is in rather good agreement with our excitation spectrum, proving the similarity of the reaction mechanism. Also the excitation spectra of both reactions for small q only (Fig. 8 and Ref. 7) are very similar: the spectra are essentially flat in the E_x-range 15-70 MeV.

Besides the comparison with $(\pi^+,2p)$, a comparison could be made with other reactions that lead to the same residual nucleus, such as (p,pd), (d,α), or (p,^{3}He). The two-nucleon pick-up reactions (d,α) and (p,^{3}He), however, are sensitive to larger recoil momenta q than the $(\pi^-,2n)$ process in our geometry.

A recent $^{12}C(p,pd)^{10}B$ measurement[25] at E_p = 75 MeV has shown about equal population of ground state and first excited state, even at recoil momentum q = 0. Their experiment showed a smaller population of the second and third excited states, similar to our results. The higher excitation region has not been measured by these authors.

Among the numerous theoretical papers on π^- absorption there are only very few that contain a detailed prediction on the excitation energy spectrum that this reaction should produce. Kopaleishvili et al.[4] have calculated this distribution for ^{12}C, among other target nuclei, assuming absorption from the atomic s-orbit and neglecting the final-state nucleon-nucleus interaction. As they show a result only for q < 50 MeV/c, our excitation spectrum for small recoil momenta (Fig. 8), should be compared with their prediction. They agree in so far as the main strength is below 5 MeV.

The latest attempt to treat the complete three-body final-state system of the $(\pi^-,2n)$ reaction by solving the corresponding Faddeev equations is the one by Garcilazo and Eisenberg[3]. In Fig. 10 a comparison between our measured ω-distribution, integrated over all E_x values, and their prediction has been made. It shows that our distribution is rather flat in the ω-range covered, and disagrees with the predicted distribution, which is peaked at 180°. If we restrict our

data to small E_s values (see Fig. 16), then the ω-distribution is peaked at this angle , and thus is in better qualitative agreement with the prediction for two nucleons coming from the $1p_{3/2}$ shell[3]. But it should be also mentioned that the shape of this shown ω-distribution depends on the choice of the upper limit in E_s, i.e. the higher this limit the less pronounced the peak at 180° generally becomes. Therefore we would like to emphasize the necessity of theoretical efforts giving more detailed excitation spectra with angular and recoil momentum distributions for certain ranges of excitation energy.

4.4 General remarks on the p-shell hole states

To discuss the systematic trends of the p-nucleon removal in different targets, the separation energy of the neutron-proton pair is more relevant than the excitation energy in the residual nuclei. In Fig. 11 our results are presented in the way that the strongly populated residual levels for ^{9}Be, ^{10}B, and ^{12}C, and also for ^{14}N [11] are indicated as a function of E_s, the separation energy of a free deuteron*). It is surprising to find that for all these targets, the peaks are nearly at the same position, namely at $E_s \sim 26$ MeV. A comparison of the energies of our $(\pi^-,2n)$ peaks and the peaks from (p,2p) results[26] as shown in Fig. 11, reveals a certain similarity between them. If the scale of the single-nucleon separation energy is expanded by almost a factor of 2 with respect to the two-nucleon separation energy, this similarity becomes obvious, and does not seem to be only fortuitous. This can be understood considering that the proton and the neutron in the same orbit are strongly correlated and can absorb the pion, whereas the correlation is weak between two nucleons from different orbits. Best agreement between the separation energies in Fig. 11 could be achieved with a multiplication factor of 1.62. It is also important to use the separation energy for the free deuteron to get this agreement.

About the quantum state of the absorbing pair the following can be said. For $\Lambda = 0$, the two components a) 2S ($\mathcal{N}= 1$, $L = 0$) × 1s ($n = 0$, $\ell = 0$) and b) 1S ($\mathcal{N}= 0$, $L = 0$) × 2s ($n = 1$, $\ell = 0$) may contribute, as has been mentioned in Section 2. For the transitions to which the c.f.p. calculations predict strong $\Lambda = 0$ contributions, such as the 7.5 MeV and 10.3 MeV levels in ^{7}Li, or the 19 MeV level in ^{8}Be, the experiment shows that the width of the corresponding q-distributions is as small as 80-90 MeV/c. This is much smaller than the width for $\Lambda = 2$ transition. In Fig. 2 a comparison with calculated q-distributions for 1S and 2S transitions is made, which shows that the above mentioned $\Lambda = 0$ transitions are closer to the 2S distribution. Therefore, the combination (a),

*) E_s is given by: $E_s = E_x + M_B - M_A + m_d$. Where M_A and M_B are the masses of the target and recoil nucleus, and m_d is the mass of the free deuteron.

corresponding to the pion absorption by a pair in a relative 1s-state, seems to be favoured compared to (b), i.e. 2s absorption.

According to our observations, for equal c.f.p., $\Lambda = 2$ transitions are generally weaker than $\Lambda = 0$ transitions. It has already been mentioned that the $L = 2$, $\ell = 0$ component of the $\Lambda = 2$ transition is suppressed in our geometry. Apparently also the second component $L = 0$, $\ell = 2$ does not appear strongly. We conclude, therefore, that the absorption by a pair in the relative d-state ($\ell = 2$) is less favoured than in the s-state ($\ell = 0$).

It should be mentioned, however, that we observe a clear though not very strong transition at 7 MeV in the residual nucleus ^{10}B, which corresponds probably to the absorption of a pair in a relative d-state, provided our attribution to a predicted $\Lambda = 2$ state is correct. The corresponding q-distribution is given in Fig. 2. It agrees with the schematically calculated distribution for a 1S-state.

5. RESULTS AND DISCUSSION -- HIGH E_x REGION

On the lithium isotopes two well-separated big peaks are observed in the excitation energy spectra obtained in the $(\pi^-,2N)$ reactions, one peak around E_x = 0-4 MeV and the other around 30 MeV [7,10,12]. The latter peak, which has more than twice the area of the former one, is interpreted as s-shell nucleon removal[7,12]. In the $^{12}C(\pi^-,2n)^{10}B$ measurement of Cheshire and Sobottka, the reported peak corresponding to s^2 removal at $E_x \sim 38$ MeV [9] is comparable in size to the p^2-removal, i.e. the ratio of s- to p-removal is smaller than in the lithium isotopes. Therefore it is interesting to look at s-nucleon removal with targets in the mass number range between lithium and carbon.

It is worth while to mention the results from (p,2p) [26] and (p,d) [27] experiments on single s-nucleon removal involving the same targets. In the corresponding separation energy spectra, a peak which is $\sim$ 20-30 MeV wide occurs at a one-nucleon separation energy of 27-34 MeV, depending on the target. In the (p,d) results, there is even some structure in this broad peak. From the analogy between p^{-1} peaks in (p,2p) results and p^{-2} peaks in $(\pi^-,2n)$ results mentioned earlier, we expect s^2-removal to appear at considerably higher E_s than one-nucleon removal. In addition, the peak should be wide, with possible fine structure.

Our excitation spectra are shown in Figs. 4, 6, 8. None of these spectra show such a clear and distinct peak at higher E_x as was observed in ^6Li or ^7Li. In ^{12}C we cannot confirm the separated s^{-2} peak, reported by Cheshire and Sobottka. This is in spite of the fact that our experimental set-up covers a much wider ω-range.

Because of the large separation energies of s-shell nucleons, one expects wide q-distributions for the corresponding peaks. In order to be more sensitive

to those states, we show in Fig. 12 the excitation spectra for events with large recoil momentum for ^{9}Be, ^{10}B, and ^{12}C, respectively. From these spectra several observations can be made. Although there is no broad, dominant peak at higher separation energies, we observe many events in this region. It should also be kept in mind that owing to the energy threshold of 15 MeV for one neutron, the high E_x-region is already somewhat suppressed. Apart from the structure at small excitation energies discussed in Section 4, structures at higher energies are visible. In the ^{12}C spectrum we recognize a peak at $E_s \sim 36.5$ MeV, followed by a dip at 42 MeV; in the case of ^{9}Be there are one or two peaks around 36 MeV and a dip at 43 MeV, and in ^{10}B a peak at 40 MeV and a dip at 45 MeV.

For the peaks just mentioned, q- and θ-distributions are shown in Fig. 13. The q-distributions are relatively wide (compared, for instance, with the 10.5 MeV peak in ^{9}Be); they increase towards q = 0 and thus indicate L = 0 dominance. The interpretation of these three narrow peaks is not simple. As the separation energies are slightly too high for p^2-removal, they might be contributions from sp-removal. The q-distributions, however, do not support this picture.

In the higher excitation-energy region, it can be expected that the contribution of mechanisms other than quasi-free 2N absorption becomes important. In fact, Favier et al.[7] estimate that in their ω-range, which is comparable to ours, half the events are due to other processes. On the other hand, our observed structure in the high excitation-energy region seems to support the quasi-free 2N process.

In order to investigate the relative contributions of these two processes, a comparison of separation energy spectra with different windows in ω and in q is shown in Figs. 14 and 15. From this comparison several remarks can be made: in the spectra with ω-windows (Fig. 14), it can be seen that for ^{9}Be, up to $E_s \sim \sim 35$ MeV, the ω-distribution is decreasing with decreasing ω, whereas beyond this point it is rather flat. For ^{12}C the distribution becomes flat at E_s = 30-37 MeV, and beyond this energy range the distribution is slightly increasing. The ^{10}B target seems to be exceptional. The ω-distribution is decreasing everywhere, although its inclination changes at $E_s \sim 34$ MeV.

In the spectra with q-windows (Fig. 15), it can be seen that the q-distribution changes rather drastically at $E_s \sim 48$ MeV for ^{12}C. Below this energy the distribution is decreasing with increasing q, whereas beyond this point it is almost flat. An indication of the same behaviour is observed in ^{9}Be. The target ^{10}B is again very different. The region where the q-distributions are decreasing continues up to $E_s \sim 70$ MeV. The sudden change of the q-distribution mentioned above can be understood if it is postulated that, at this separation energy, s^2-removal replaces p^2-removal. In the latter case, according to our observation, the

dominant transitions come from 2S ($\mathcal{N}$ = 1, L = 0), showing a narrow q-distribution. In the case of s^2-removal, however, only transitions corresponding to 1S ($\mathcal{N}$ = 0, L = 0) are allowed. This causes a considerably wider q-distribution, in addition to the widening of the q-distribution owing to the larger separation energy.

The processes other than the quasi-free 2N absorption are expected to produce distributions that do not critically depend on the target nucleus, if the mass is similar. In the separation energy spectra for q-windows as well as for ω-windows, ^{10}B is very different from the other targets. This difference can also be seen in the ω distributions for the range of separation energies between 48 MeV and 70 MeV, as shown in Fig. 16. It seems therefore not very likely that processes other than quasi-free 2N absorption are dominant in this energy range.

This conclusion is also supported by the absolute rates. In Table 1 the integrated rates per stopped pion for the low E_s-region as well as for the high E_s-region are given for all three target nuclei. The numbers correspond to the ω-range from 145° to 180°. In the low E_x-region the observed ω-distributions are strongly peaked at 180° and hence our set-up covers nearly all events. This is certainly no longer the case in the high E_x-region, because there the ω-distributions are much wider. An isotropic ω-distribution, however, can be excluded, because in this case the extrapolated rates per stopped pion integrated over all the ω-range would far exceed 100%. A non-isotropic ω-distribution can in turn be more easily explained by direct processes.

6. CONCLUSIONS

It was shown that for all three targets, ^{9}Be, ^{10}B, ^{12}C, studied in our experiment, the prominent peaks in the low excitation-energy region can be attributed to known levels, and that their population is in a qualitative agreement with the c.f.p. calculations for the p-shell nucleons.

In these target nuclei, as well as in ^{14}N, a surprising similarity has been found between the systematics of the two-nucleon separation energy E_s of the two-hole states strongly populated in the $(\pi^-,2n)$ reaction, and the one-nucleon separation energy of the single-hole states observed in the (p,2p) reaction. This could be explained by a strong correlation between proton and neutron in the same orbit.

For the p^2-removal, the small width of the q-distributions for Λ = 0 transitions and the general weakness of Λ = 2 transitions seem to indicate that the pion absorption by a nucleon pair in relative 1s-state is favoured compared to the 2s- as well as the 1d-states.

Relatively high rates have been observed for the transitions leading to high separation energies. Although no quantitative conclusion on the relative

contribution of s^2-removal and non-quasi-free 2N processes could be made, the absolute rate corresponding to this E_s region in our ω-range, as well as the structure observed in the excitation spectra, seem to support the importance of the s^{-2} process.

A comparison between our excitation spectra and those from the low-energy $(\pi^+,2p)$ reaction shows that, within the experimental precision, the relative population of the residual levels is very similar in these reactions. For the nuclei studied here, we conclude therefore that the relative population does not depend on whether the pion is absorbed from atomic orbits or in flight.

Acknowledgements

We would like to express our thanks to all the members of the SC group for their collaboration, and in particular to Dr. E.G. Michaelis, who also carefully read the manuscript.

Table 1

Integrated rates per stopped pion for different E_s-regions. The numbers are corrected with respect to geometrical efficiencies in the ω-range between 145° and 180°.

	E_s < 35 MeV	E_s > 35 MeV
^{9}Be	14.5%	22%
^{10}B	12.5%	16%
^{12}C	10%	16%

REFERENCES

1) T. Ericson, Phys. Letters 2, 278 (1962).

2) J.W. Morris and H.J. Weber, Ann. Phys. (USA) 79, 34 (1973).

3) H. Garcilazo and J.M. Eisenberg, Nuclear Phys. A220, 13 (1974).

4) T.I. Kopaleishvili, I.Z. Machabeli and M.Sh. Chachkhunashvili, Soviet J. Nuclear Phys. 15, 629 (1972).

5) C. Cohen and D. Kurath, Nuclear Phys. A141, 145 (1970).

6) V.V. Balashov, A.N. Boyarkina and I. Rotter, Nuclear Phys. 59, 417 (1964).

7) J. Favier, T. Bressani, G. Charpak, L. Massonnet, W.E. Meyerhof and Č. Zupančič, Nuclear Phys. A169, 540 (1971).

8) E.D. Arthur, W.C. Lam, J. Amato, D. Axen, R.L. Burman, P. Fessenden, R. Macek, J. Oostens, W. Shlaer, S. Sobottka, M. Salomon and W. Swenson, Phys. Rev. C 11, 332 (1975).

9) D.L. Cheshire and S.E. Sobottka, Nuclear Phys. A146, 129 (1970).

10) F. Calligaris, C. Cernigoi, I. Gabrielli and F. Pellegrini, Nuclear Phys. A126, 209 (1969).

11) B. Bassalleck, H.D. Engelhardt, M. Furić, E.L. Haase, W.D. Klotz, C.W. Lewis, F. Takeutchi and H. Ullrich, Phys. Letters 65B, 128 (1976).

12) R.L. Burman and M.E. Nordberg, Jr., Phys. Rev. Letters 21, 229 (1968).

13) B. Bassalleck, D. Engelhardt, M. Furić, W.-D. Klotz, C.W. Lewis, F. Takeutchi and H. Ullrich, Meson-Nuclear Physics 1976 (eds. P.D. Barnes et al.) (AIP, New York, 1976), p. 272.

14) D.S. Koltun, Phys. Rev. 162, 962 (1967).

15) Y. Sakamoto, P. Cüer and F. Takeutchi, Phys. Rev. C 11, 668 (1975).

16) F. Takeutchi, B. Kober and E.L. Haase, Two-neutron emission induced by stopped π^- on ^{9}Be, ^{10}B, and ^{12}C, CERN preprint, 1 July 1975, presented at the Journées d'étude de physique nucléaire à moyennes énergies, IPN, Orsay, 1975.

17) R.J. Kurz, UCRL-11339 (1964).

18) F.C. Barker, Nuclear Phys. 83, 418 (1966).

19) C. Détraz, J. Cerny and R.H. Pehl, Phys. Rev. Letters 14, 708 (1965); J. Cerny, C. Détraz and R.H. Pehl, Phys. Rev. 152, 950 (1966).

20) S. Meshkov and C.W. Ufford, Phys. Rev. 101, 734 (1956).

21) F. Ajzenberg-Selove and T. Lauritsen, Nuclear Phys. A227, 1 (1974).

22) S. Ozaki, R. Weinstein, O. Glass, E. Lock, L. Neimala and A. Wattenberg, Phys. Rev. Letters 4, 533 (1960).

23) M.E. Nordberg, K.F. Kinsey and R.L. Burman, Phys. Rev. 165, 1096 (1968).

24) H.O. Funsten, W.J. Kossler and C.E. Stronach, Bull. APS 17, Ser. 2, 464 (1972).

25) J.-Y. Grossiord, Thesis, Université de Lyon (1976).

26) G. Jacob and A.J. Maris, Rev. Mod. Phys. 38, 121 (1966), and references therein.

27) B. Fagerström and J. Källne, Phys. Scripta 8, 14 (1973).

Figure captions

Fig. 1 : Kinematical variables used in the text.

Fig. 2 : Recoil momentum distributions as measured for the 10.5 MeV level in ^{7}Li (O), and for the 7 MeV level in ^{10}B (●). The curves correspond to 1S, 2S, and 1D c.m. states and are calculated in the same manner as described in Ref. 15. A square well potential has been used, and the parameter in the n-p relative wave function is chosen according to the electron scattering data.

Fig. 3 : Experimental set-up. For details see text.

Fig. 4 : Excitation energy spectrum for the residual nucleus ^{7}Li. Upper curve: all data; lower curve: events with $q < 100$ MeV/c.

Fig. 5 : q- and θ-distributions for three peaks in the E_x spectrum of ^{7}Li. For the θ-distributions, q has been restricted to less than 220 MeV/c, 210 MeV/c, and 200 MeV/c from top to bottom.

Fig. 6 : Excitation energy spectrum for the residual nucleus ^{8}Be. Upper curve: all data; middle curve: events with $q < 100$ MeV/c; lower curve: events with $q > 140$ MeV/c. Results of c.f.p. calculations from Ref. 5 (CK) and Ref. 6 (BBR) are indicated on top of the figure. For (CK) the solid lines refer to $T = 0$ and dashed lines to $T = 1$. For (BBR), solid lines refer to $\Lambda = 2$, $T = 0$, and the dashed line to $\Lambda = 0$, $T = 0$.

Fig. 7 : q- and θ-distributions for two peaks in the E_x-spectrum of ^{8}Be. For the θ-distributions, q has been restricted to less than 190 MeV/c and 170 MeV/c for the lower and higher E_x-window, respectively.

Fig. 8 : Excitation energy spectrum for the residual nucleus ^{10}B. Upper curve: all data; lower curve: events with $q < 100$ MeV/c. Results of c.f.p. calculations from Ref. 5 (CK) and Ref. 6 (BBR) for $T = 0$ (solid lines) and $T = 1$ (dashed lines) are indicated on top of the figure.

Fig. 9 : q- and θ-distributions for three peaks in the E_x spectrum of ^{10}B. For the θ-distributions, q has been restricted to less than 180 MeV/c, 170 MeV/c, and 165 MeV/c from top to bottom.

Fig. 10 : Measured (●) ω-distribution from the reaction $^{12}C(\pi^-,2n)^{10}B$, integrated over all E_x, compared with the theoretical prediction (curve) of Ref. 3 with correlation parameter $r_c = 0.6$ fm. The two distributions have been normalized at 180°.

Fig. 11 : Comparison of separation energies for the removal of one (dashed lines) and two (solid lines) nucleons for the three targets measured in this experiment and for ^{14}N from Ref. 11.

Fig. 12 : Comparison of E_s spectra with q > 140 MeV/c for the three targets. E_x scales are also shown.

Fig. 13 : q- and θ-distributions for three peaks in the intermediate E_x-region. For the θ-distributions, q has been restricted to less than 160 MeV/c.

Fig. 14 : Separation energy spectra for different ω-windows for the three targets. Curves I to V correspond to windows in (-cos ω) of 0.820-0.856; 0.856-0.892; 0.892-0.928; 0.928-0.964, and 0.964-1.00, respectively.

Fig. 15 : Separation energy spectra for different q-windows for the three targets.

Fig. 16 : Comparison of ω-distributions for the three targets, for small and large separation energies.

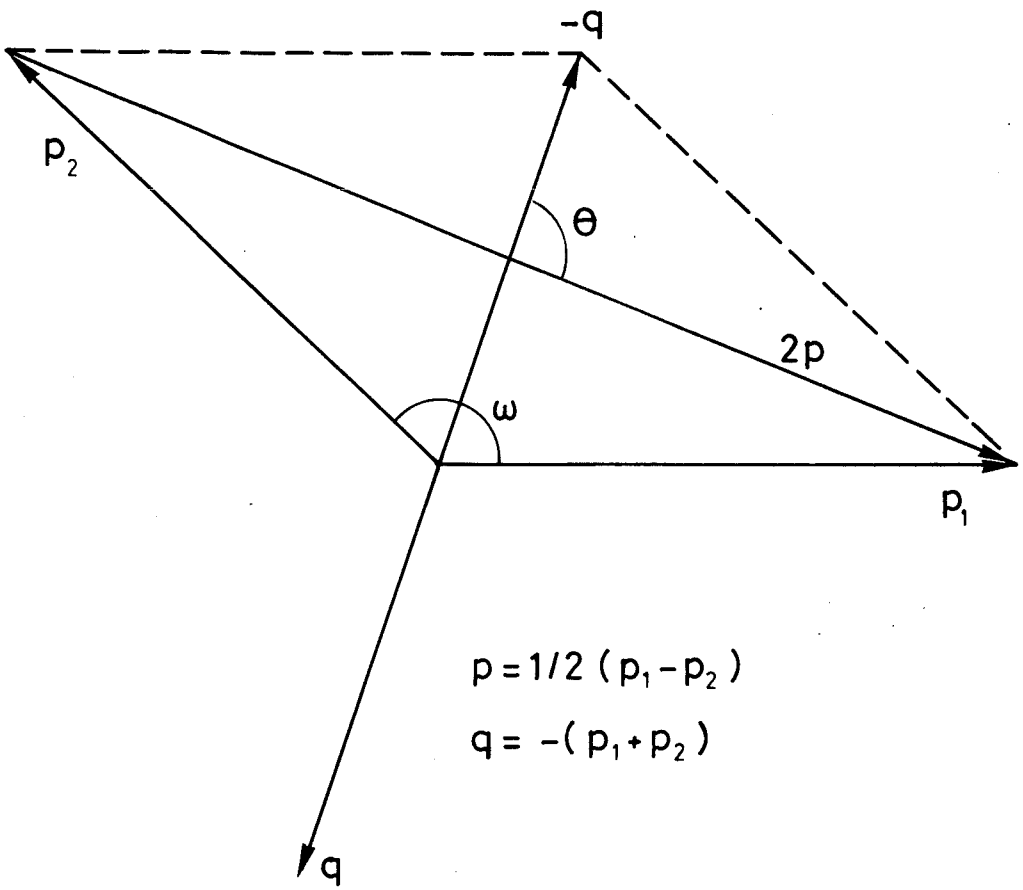

Fig. 1

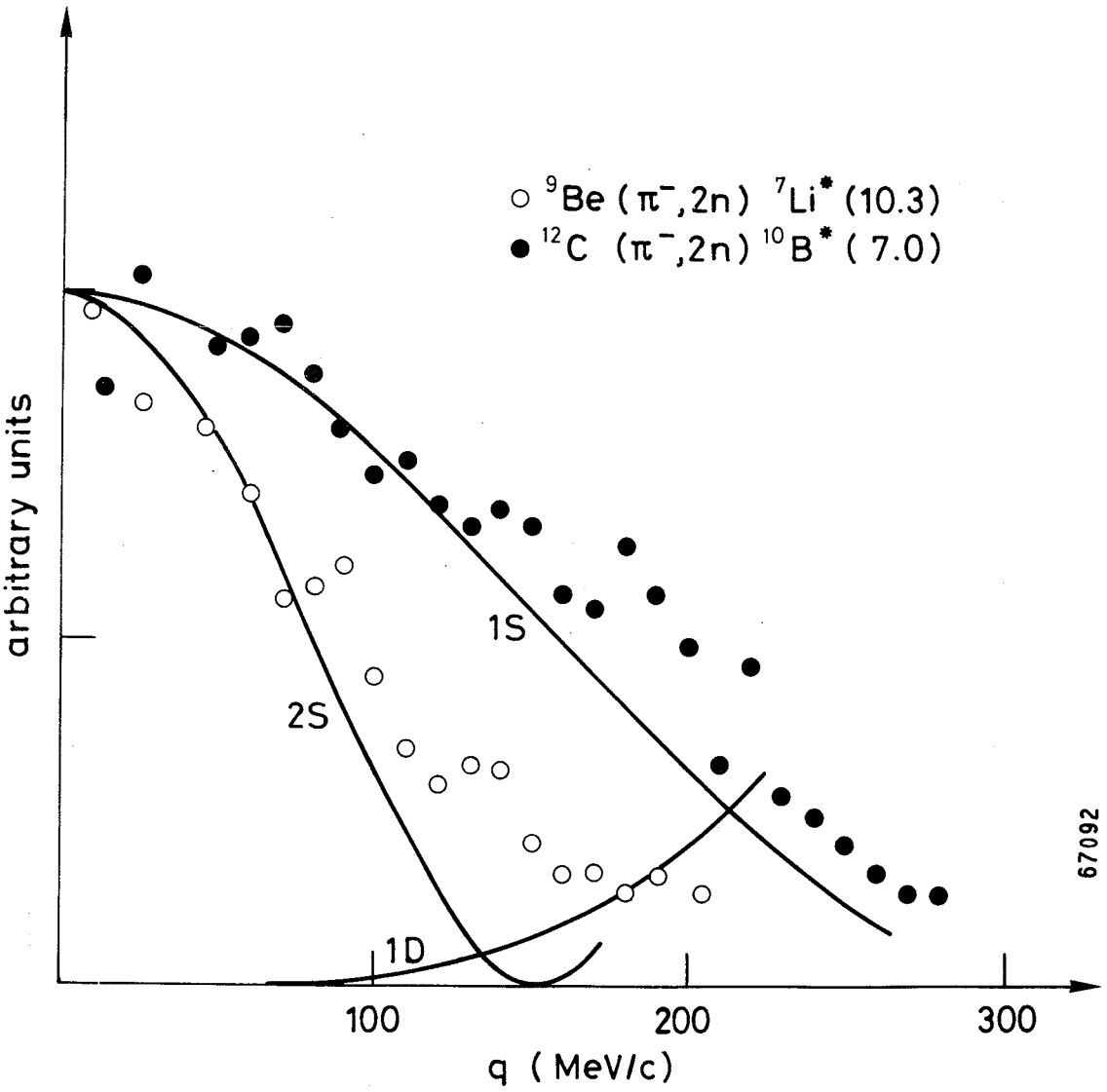
○ ^{9}Be (π⁻, 2n) ^{7}Li* (10.3)
● ^{12}C (π⁻, 2n) ^{10}B* (7.0)
arbitrary units
1S
2S
1D
100
200
300
q (MeV/c)
67092

Fig. 2

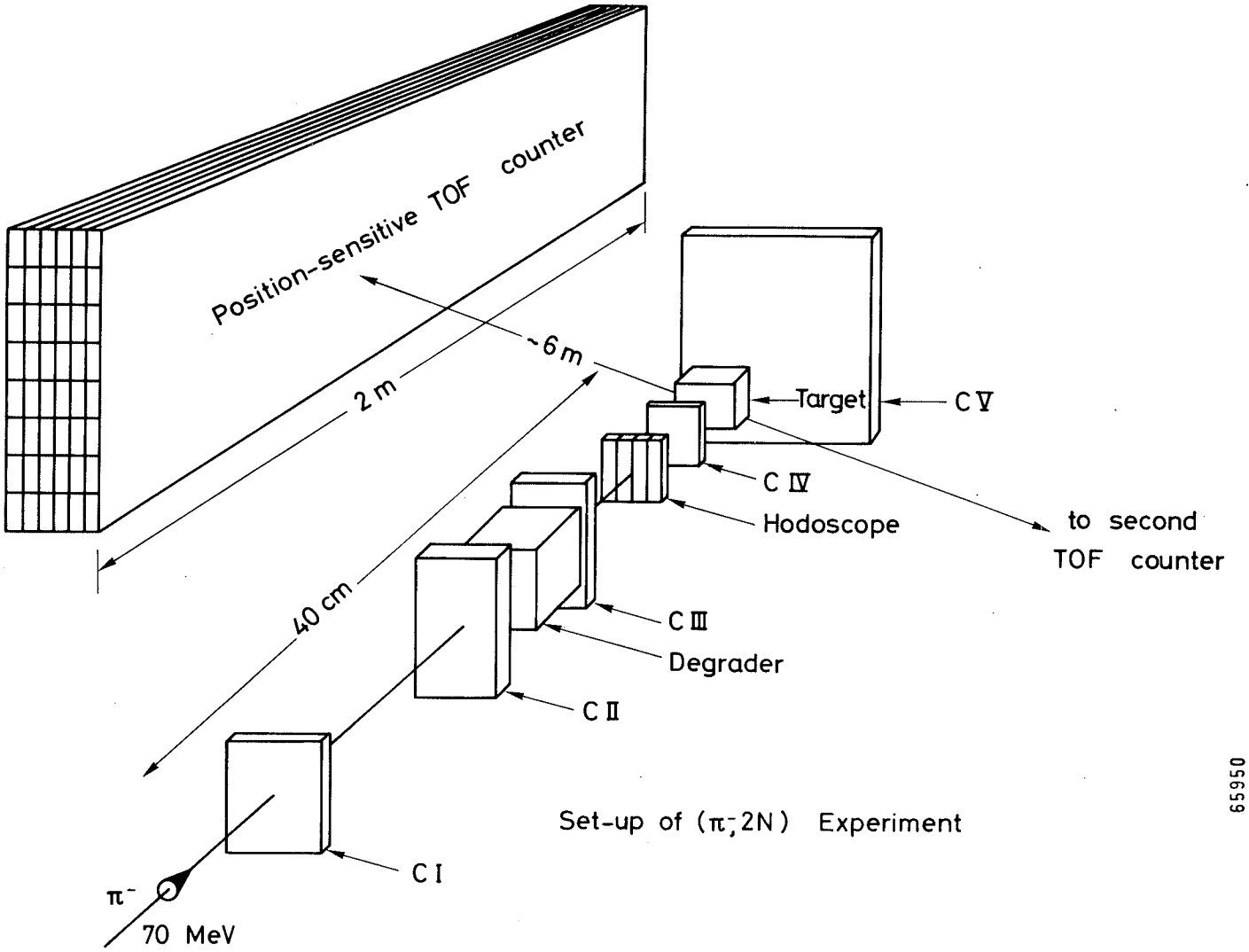

Set-up of $(\pi^-, 2N)$ Experiment

Fig. 3

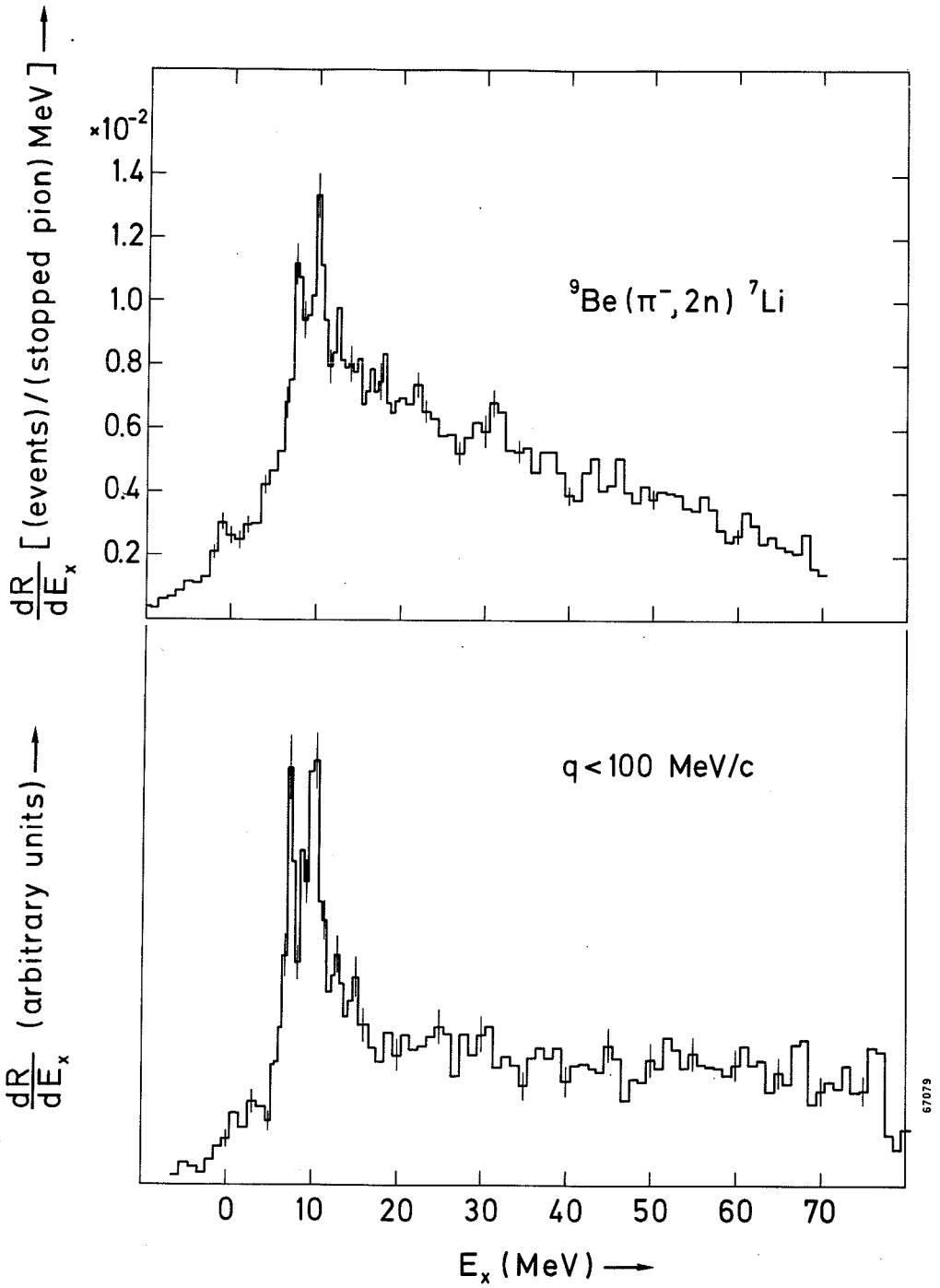
$\frac{dR}{dE_x}$ [(events)/(stopped pion) MeV] ⟶
×10⁻²
1.4
1.2
1.0
0.8
0.6
0.4
0.2
⁹Be(π⁻, 2n) ⁷Li
q < 100 MeV/c
$\frac{dR}{dE_x}$ (arbitrary units) ⟶
0
10
20
30
40
50
60
70
E_x (MeV) ⟶
67079

Fig. 4

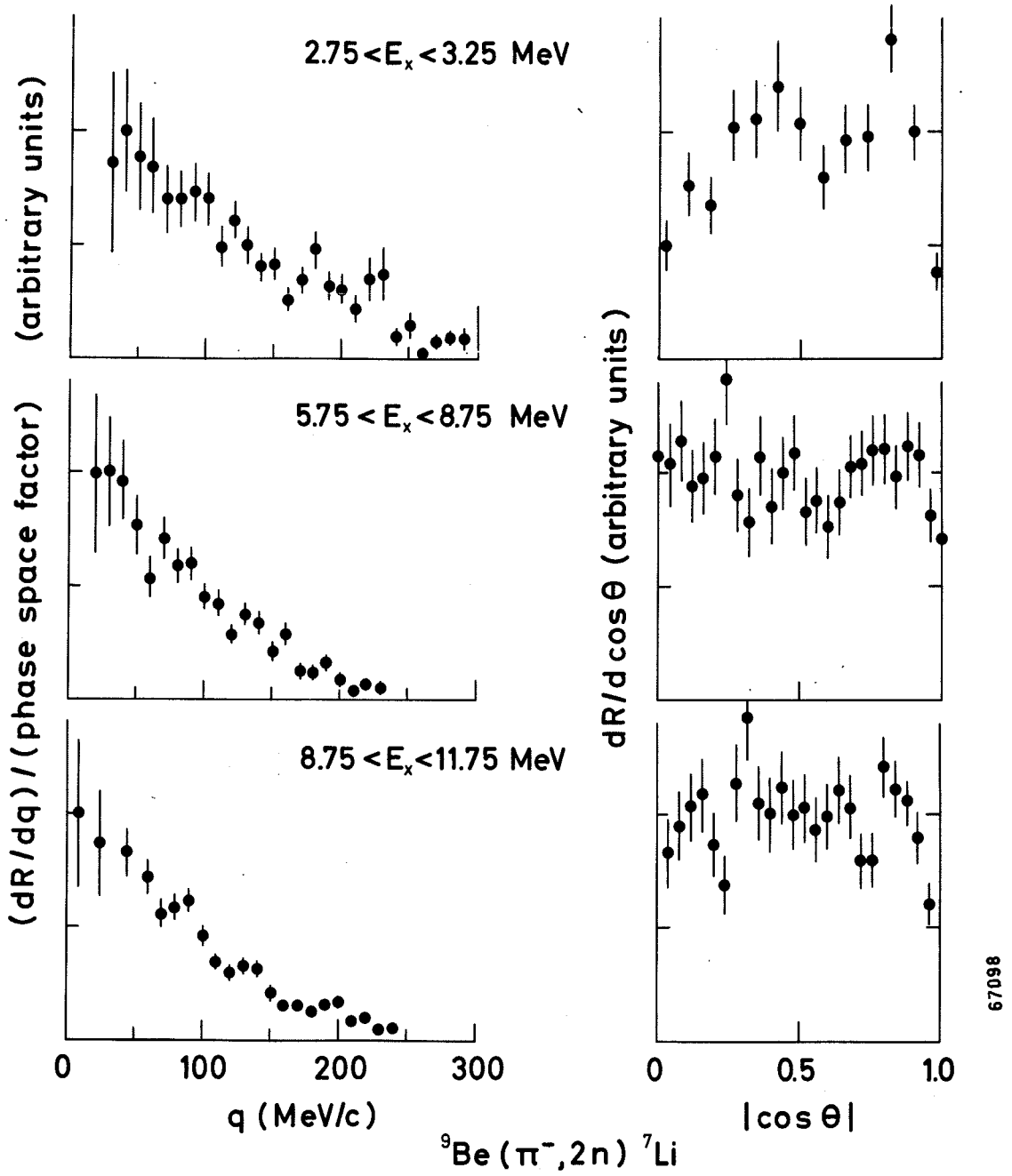
2.75 < E_x < 3.25 MeV
5.75 < E_x < 8.75 MeV
8.75 < E_x < 11.75 MeV
(dR/dq) / (phase space factor) (arbitrary units)
dR/d cos θ (arbitrary units)
0
100
200
300
q (MeV/c)
0
0.5
1.0
|cos θ|
67098
9Be (π⁻, 2n) 7Li

Fig. 5

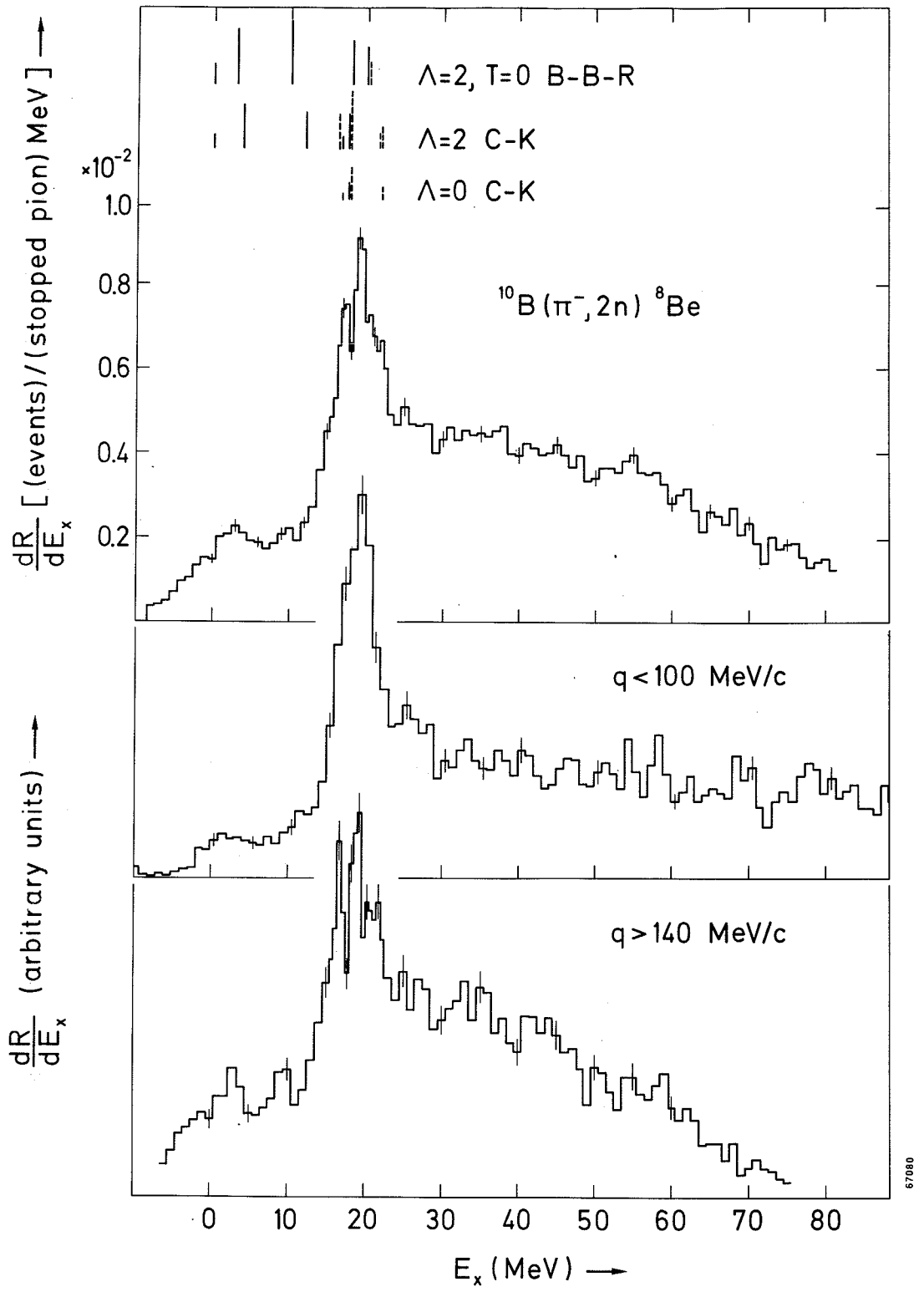
Λ=2, T=0 B-B-R
Λ=2 C-K
Λ=0 C-K
×10⁻²
1.0
0.8
0.6
0.4
0.2
¹⁰B (π⁻, 2n) ⁸Be
dR/dE_x [(events)/(stopped pion) MeV] →
q < 100 MeV/c
q > 140 MeV/c
dR/dE_x (arbitrary units) →
0
10
20
30
40
50
60
70
80
E_x (MeV) →
67080

Fig. 6

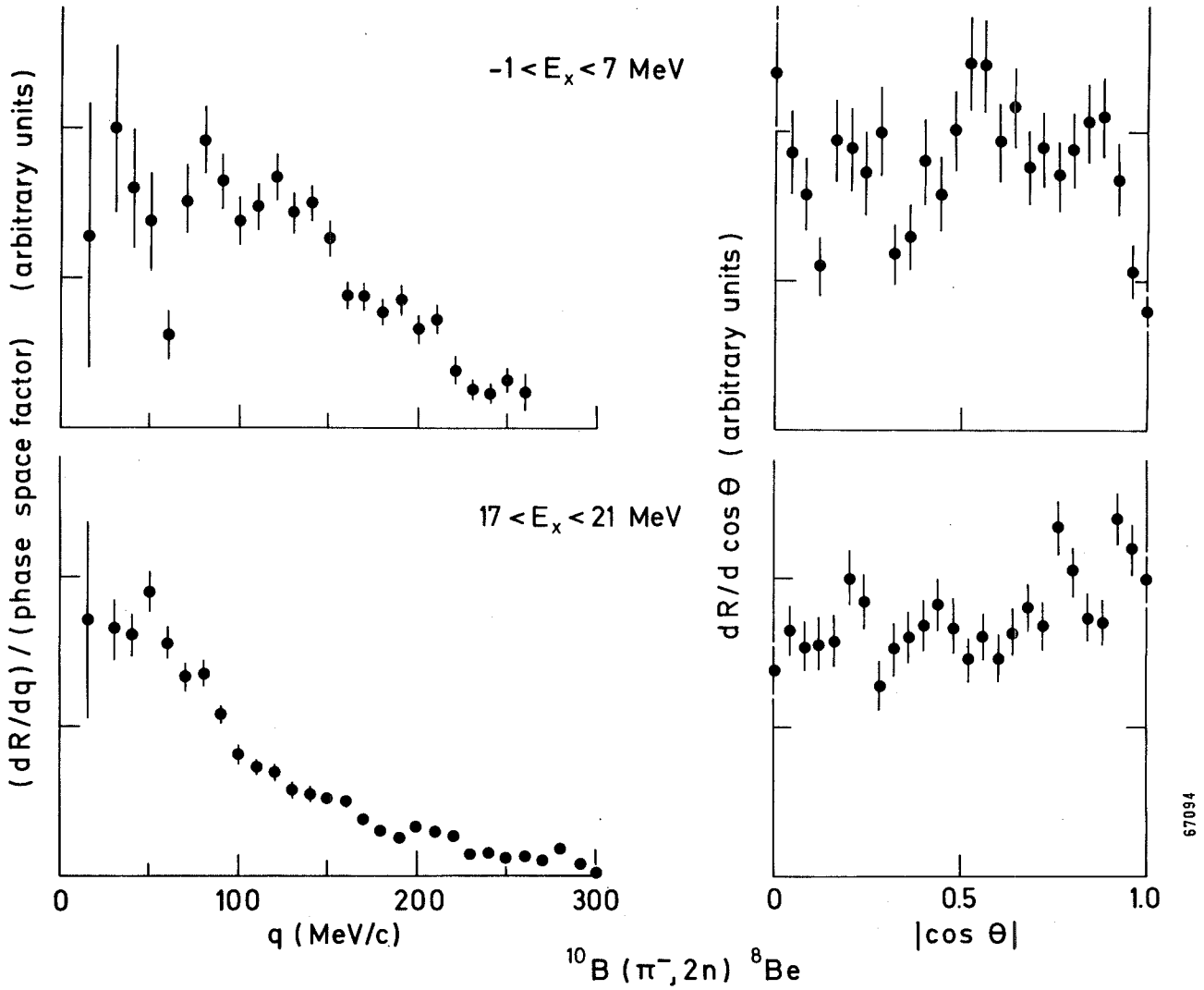
-1 < E_x < 7 MeV
17 < E_x < 21 MeV
(dR/dq) / (phase space factor) (arbitrary units)
dR/d cos Θ (arbitrary units)
0
100
200
300
q (MeV/c)
0
0.5
1.0
|cos Θ|
67094
10B (π⁻, 2n) 8Be

Fig. 7

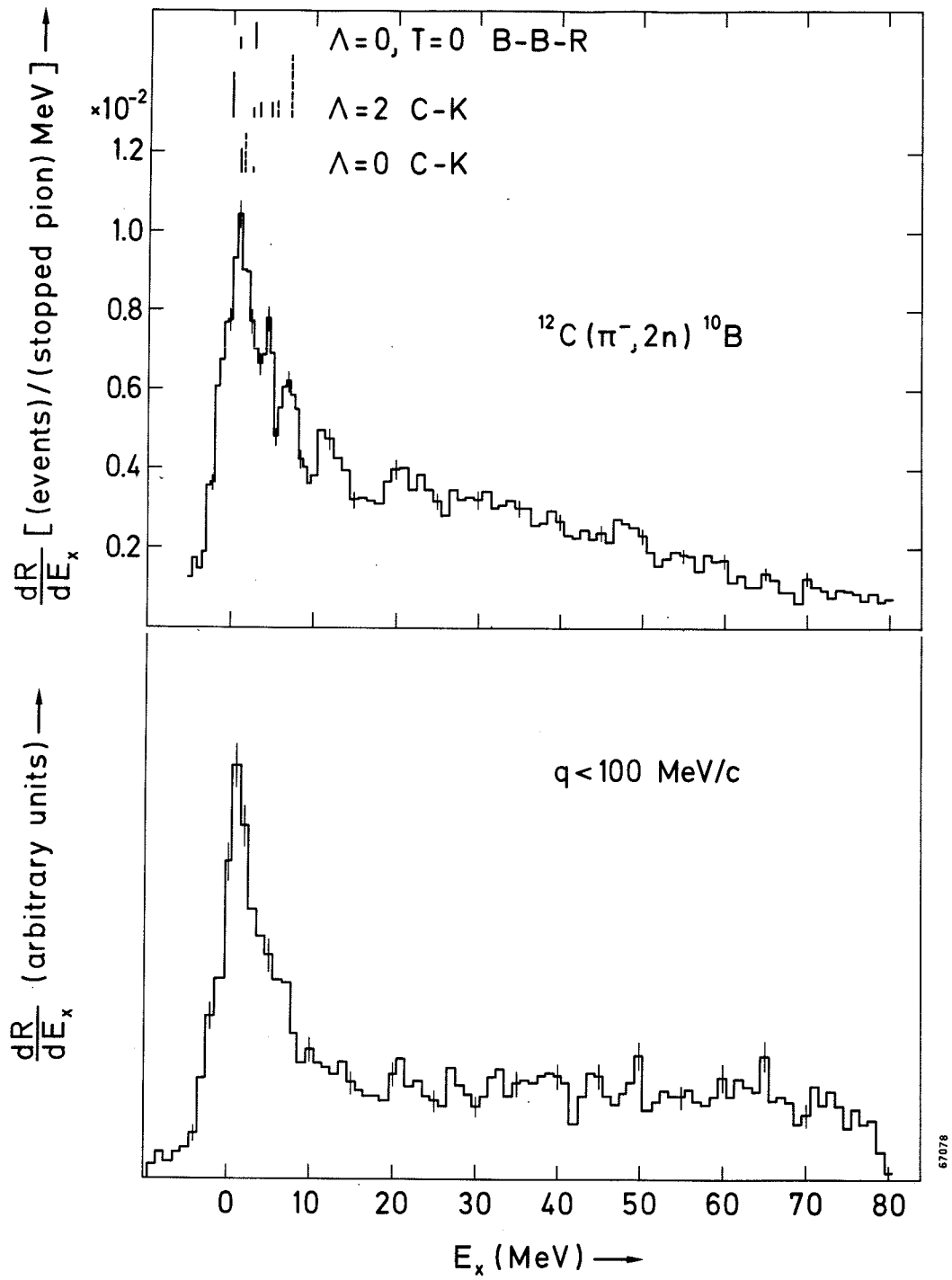
Λ=0, T=0 B-B-R
Λ=2 C-K
Λ=0 C-K
×10⁻²
1.2
1.0
0.8
0.6
0.4
0.2
dR/dE_x [(events)/(stopped pion) MeV]
¹²C (π⁻, 2n) ¹⁰B
q<100 MeV/c
dR/dE_x (arbitrary units)
0
10
20
30
40
50
60
70
80
E_x (MeV)
67078

Fig. 8

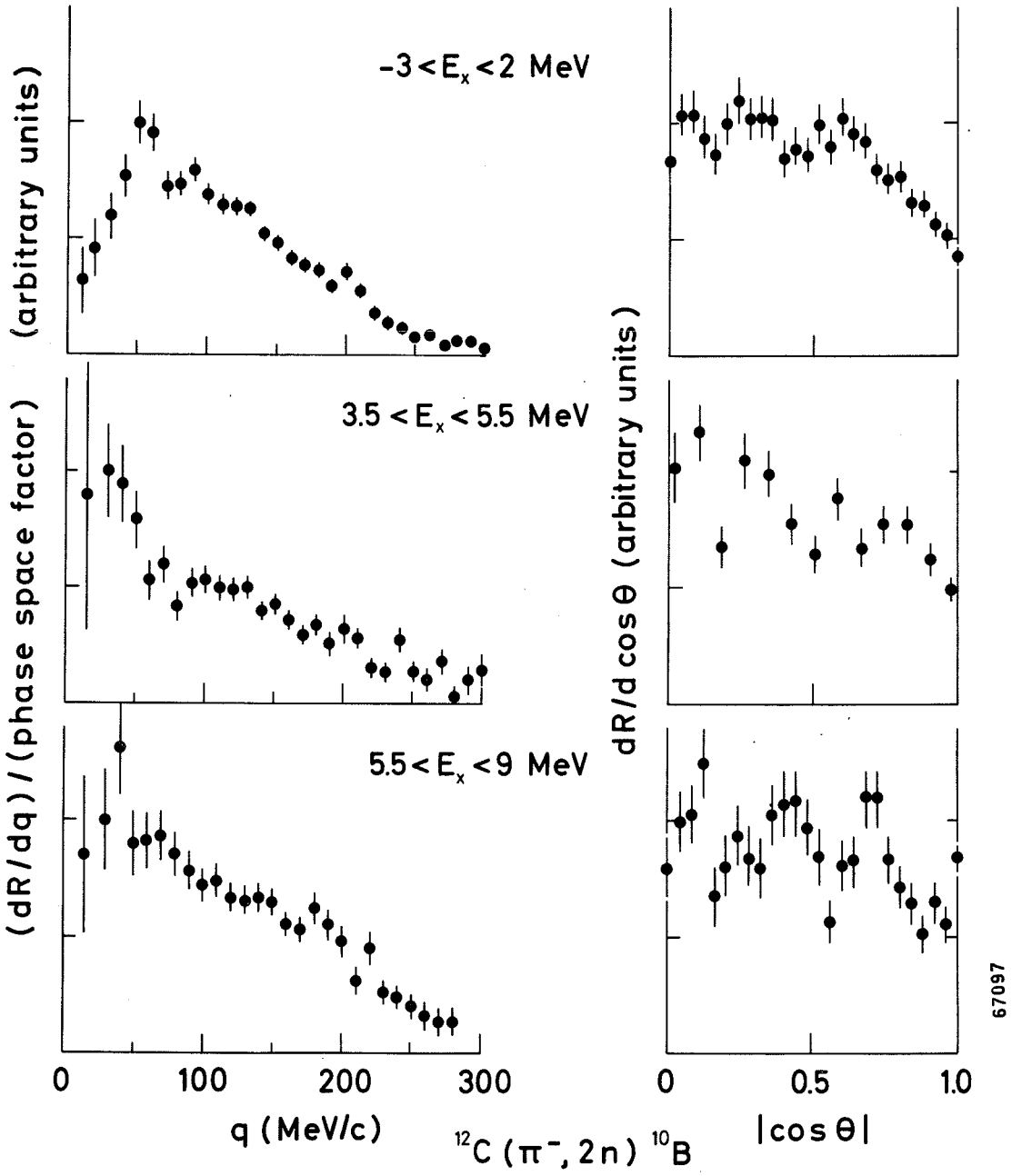
-3 < E_x < 2 MeV
3.5 < E_x < 5.5 MeV
5.5 < E_x < 9 MeV
(dR/dq) / (phase space factor) (arbitrary units)
dR/d cos θ (arbitrary units)
0
100
200
300
q (MeV/c)
0
0.5
1.0
|cos θ|
12C (π⁻, 2n) 10B
67097

Fig. 9

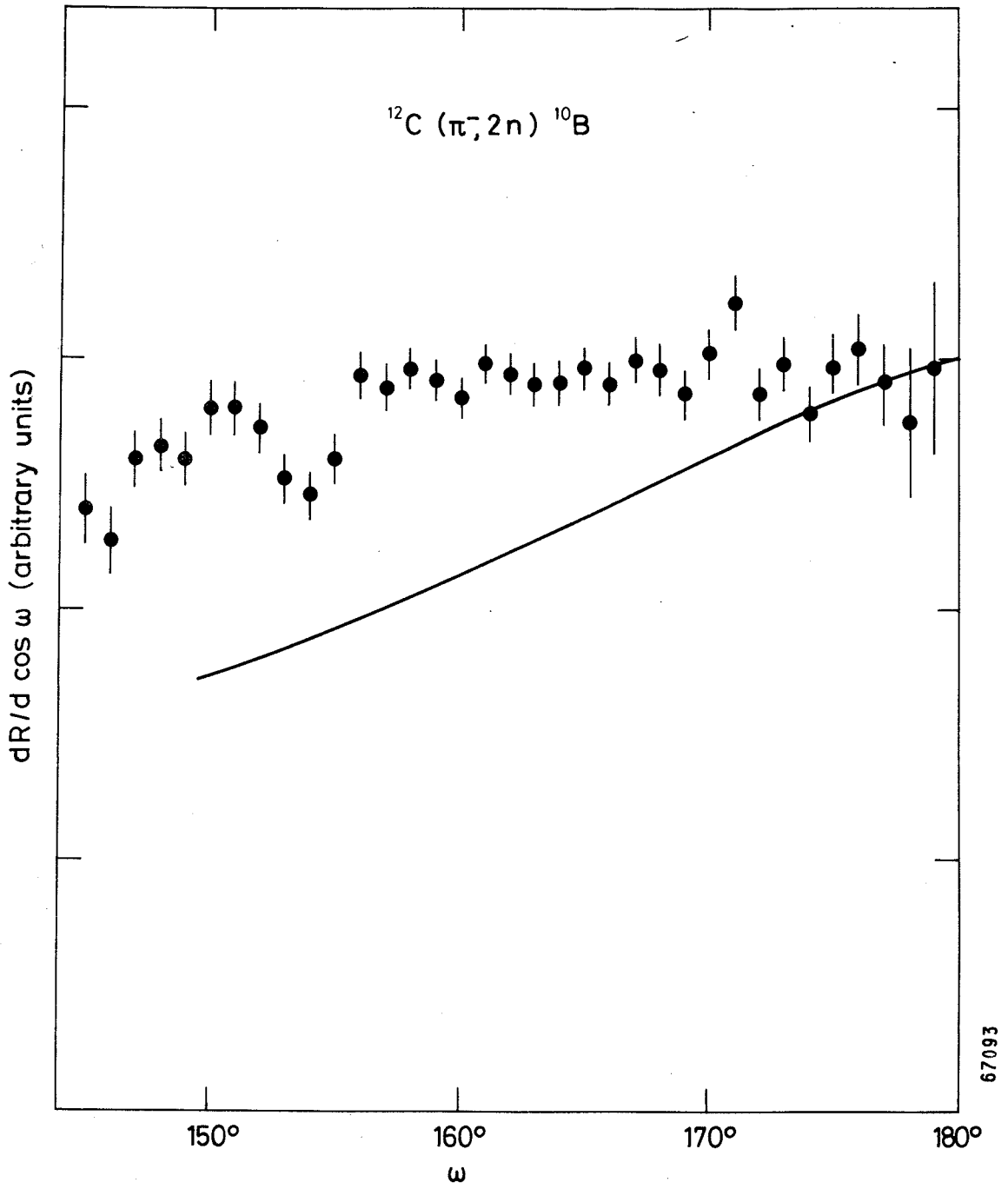

Fig. 10

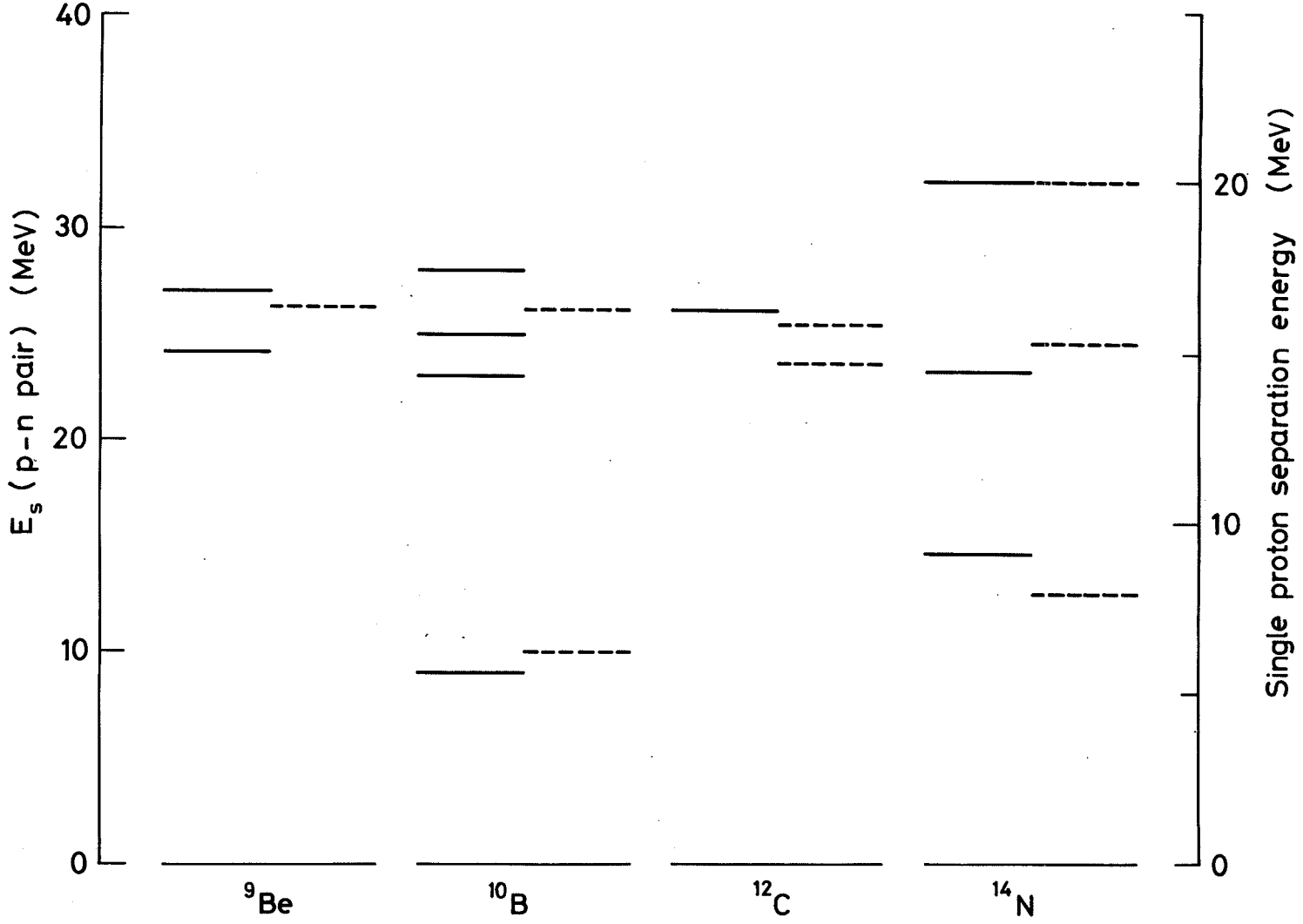
40
30
20
10
0
E_s (p-n pair) (MeV)
20
10
0
Single proton separation energy (MeV)
^{9}Be
^{10}B
^{12}C
^{14}N

Fig. 11

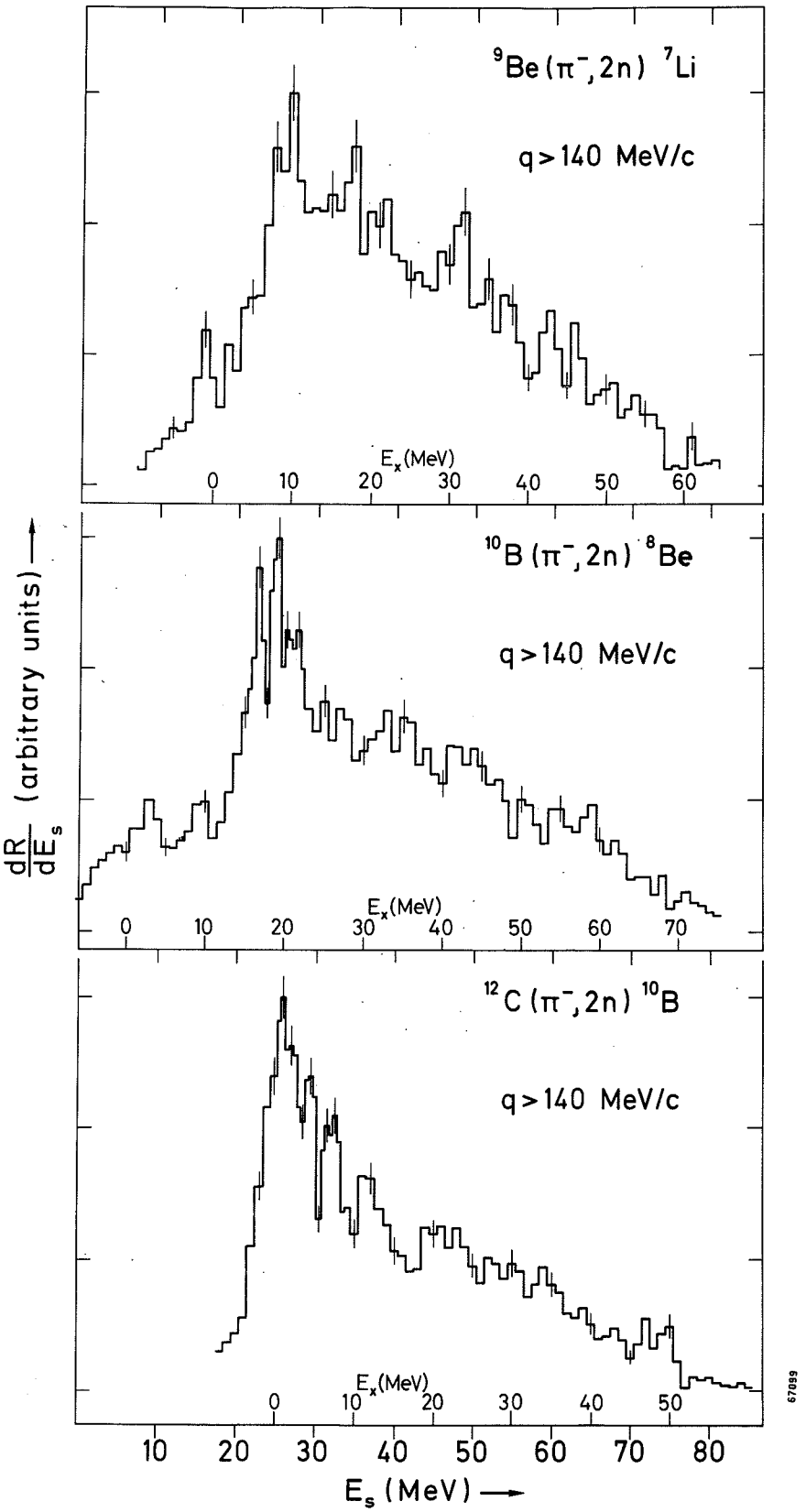
$^{9}Be(\pi^-,2n)\ ^{7}Li$
q>140 MeV/c
E_x(MeV)
0 10 20 30 40 50 60
$^{10}B(\pi^-,2n)\ ^{8}Be$
q>140 MeV/c
E_x(MeV)
0 10 20 30 40 50 60 70
$^{12}C(\pi^-,2n)\ ^{10}B$
q>140 MeV/c
E_x(MeV)
0 10 20 30 40 50
$\frac{dR}{dE_s}$ (arbitrary units) ⟶
10 20 30 40 50 60 70 80
E_s (MeV) ⟶
67089

Fig. 12

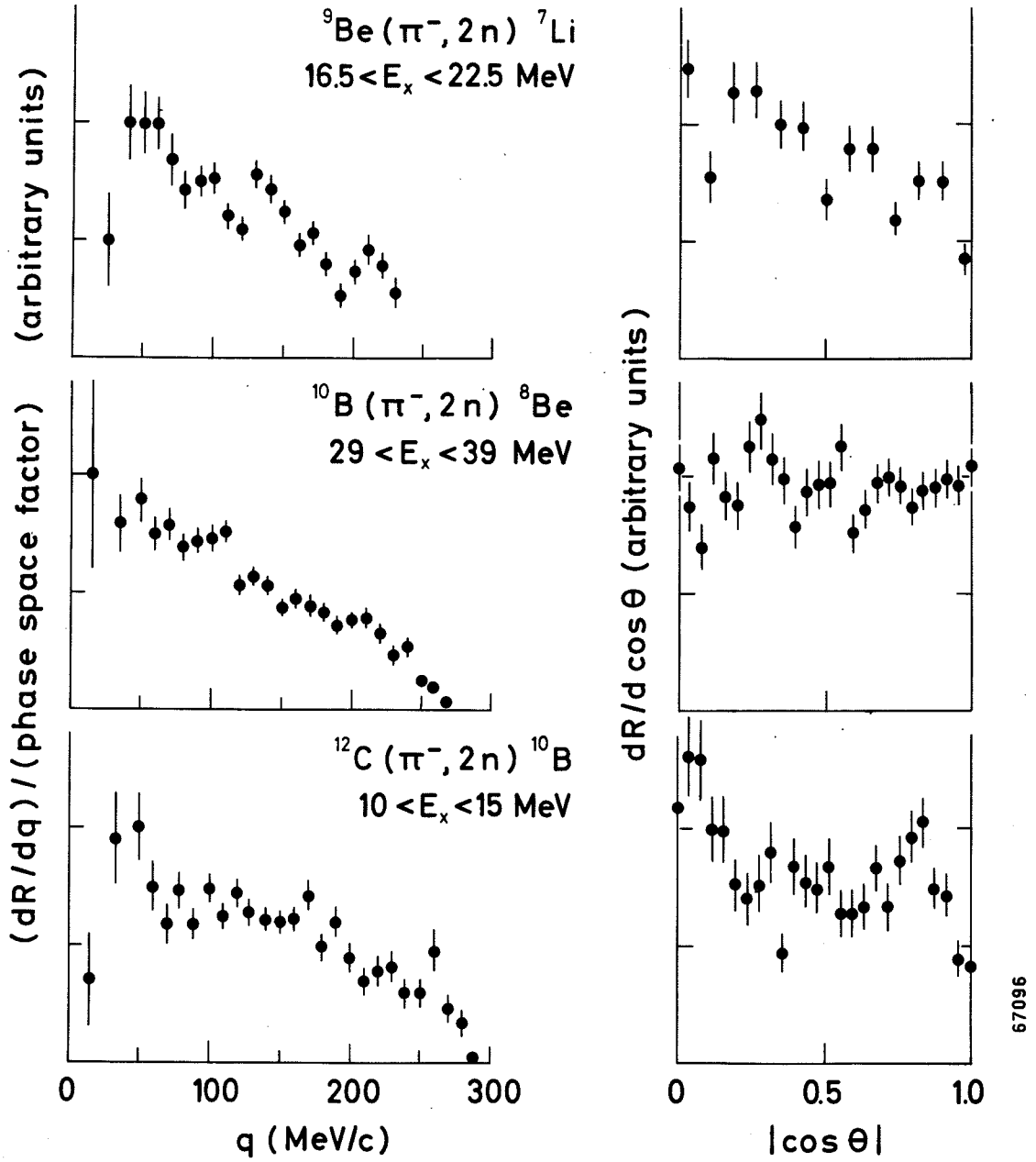
$^{9}Be(\pi^-, 2n)\ ^{7}Li$
$16.5 < E_x < 22.5$ MeV
$^{10}B(\pi^-, 2n)\ ^{8}Be$
$29 < E_x < 39$ MeV
$^{12}C(\pi^-, 2n)\ ^{10}B$
$10 < E_x < 15$ MeV
(dR/dq) / (phase space factor) (arbitrary units)
dR/d cos θ (arbitrary units)
0
100
200
300
q (MeV/c)
0
0.5
1.0
|cos θ|
67096

Fig. 13

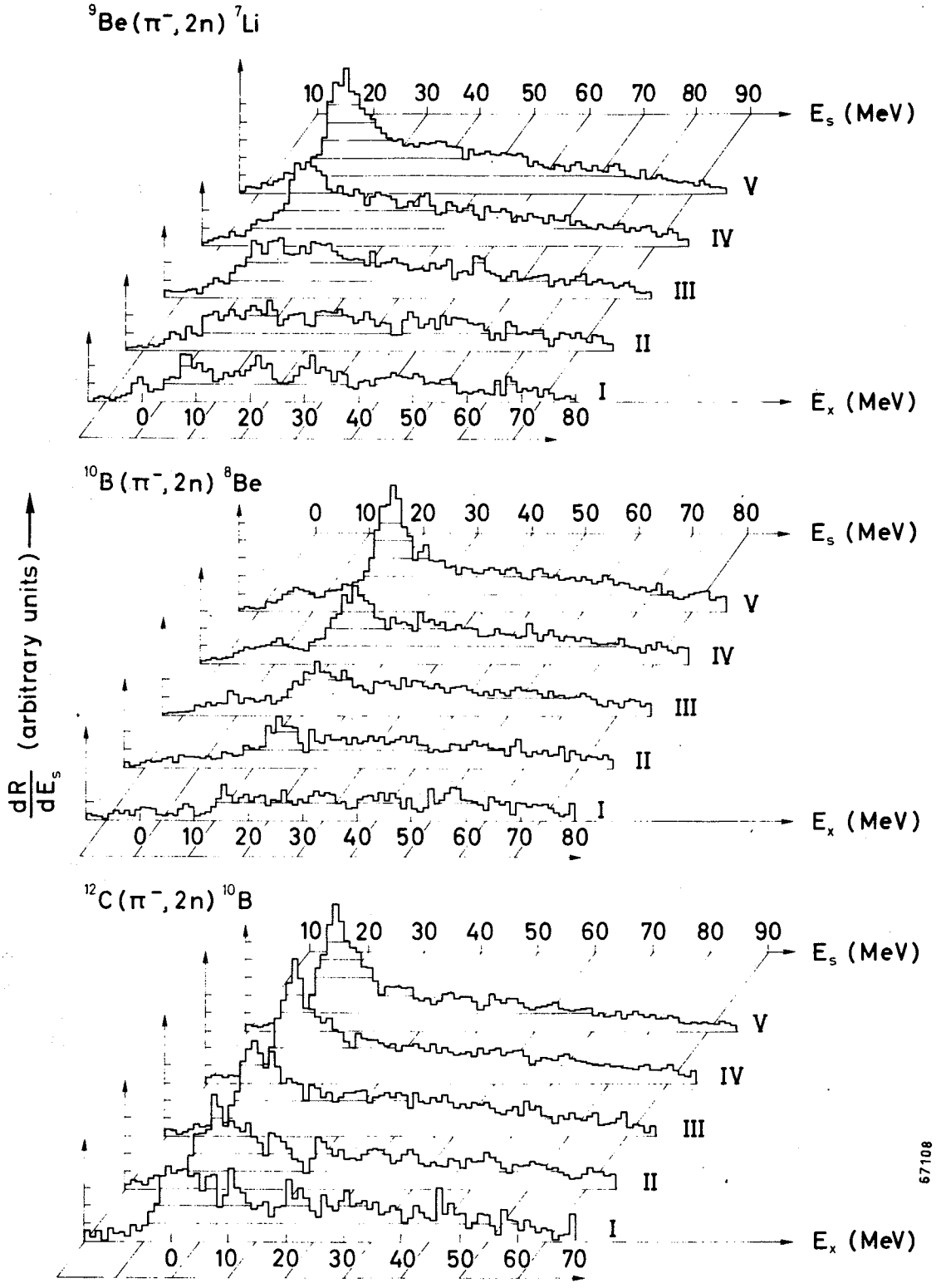
$^{9}Be(\pi^-, 2n)\,^{7}Li$
$^{10}B(\pi^-, 2n)\,^{8}Be$
$^{12}C(\pi^-, 2n)\,^{10}B$
$\frac{dR}{dE_s}$ (arbitrary units)
E_s (MeV)
E_x (MeV)
I
II
III
IV
V
67108

Fig. 14

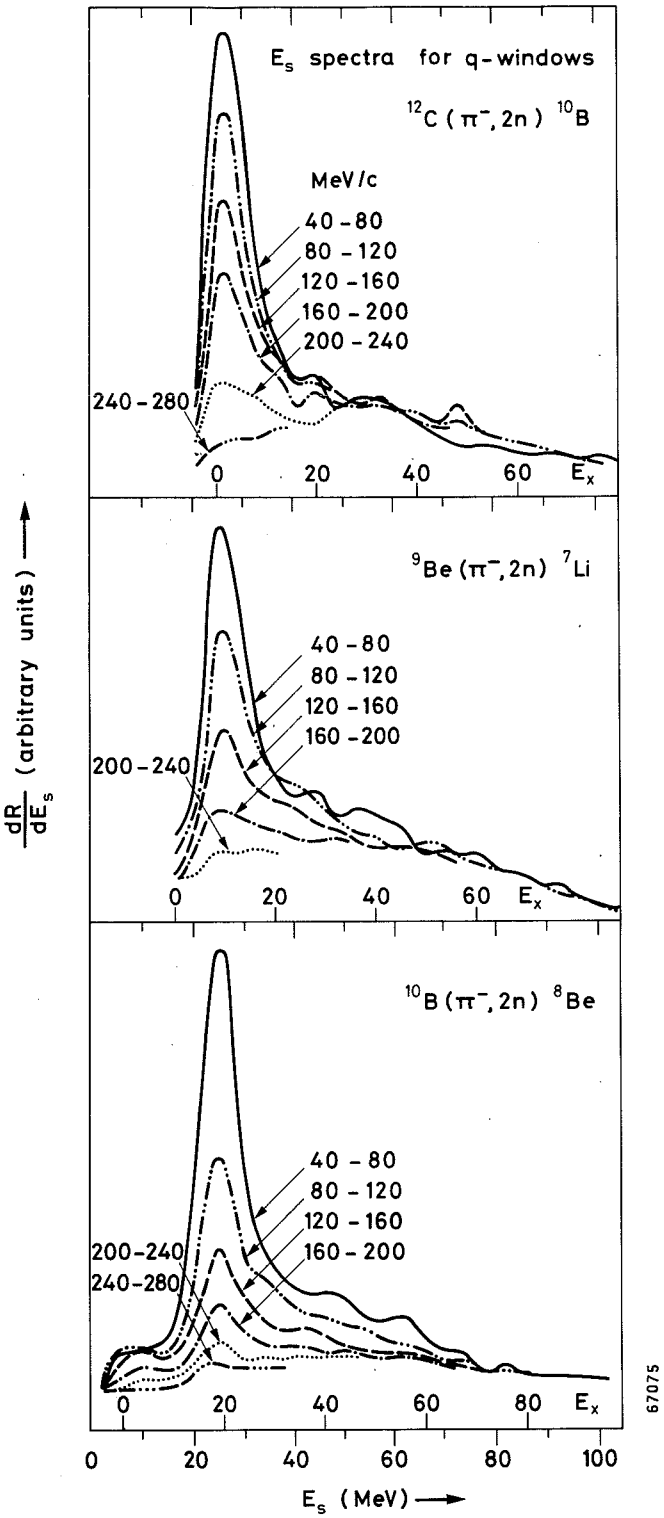
E_s spectra for q-windows
$^{12}C(\pi^-, 2n)\ ^{10}B$
MeV/c
40 - 80
80 - 120
120 - 160
160 - 200
200 - 240
240 - 280
$^{9}Be(\pi^-, 2n)\ ^{7}Li$
40 - 80
80 - 120
120 - 160
160 - 200
200 - 240
$^{10}B(\pi^-, 2n)\ ^{8}Be$
40 - 80
80 - 120
120 - 160
160 - 200
200 - 240
240 - 280
E_x
$\frac{dR}{dE_s}$ (arbitrary units)
E_s (MeV)
67075

Fig. 15

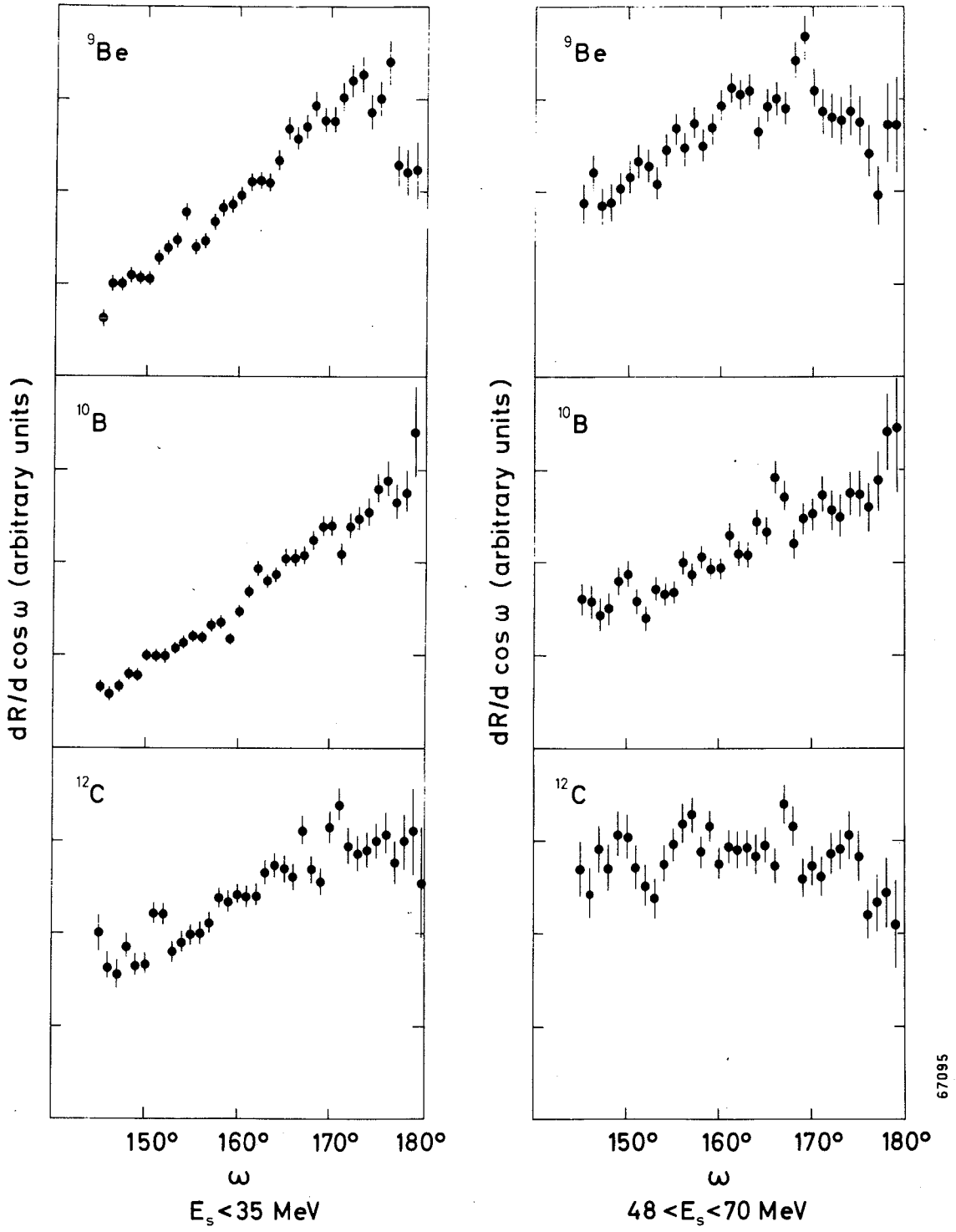
^{9}Be
^{10}B
^{12}C
dR/d cos ω (arbitrary units)
150°
160°
170°
180°
ω
E_s < 35 MeV
48 < E_s < 70 MeV
67095

Fig. 16